

Homogenized limit analysis of masonry structures with random input properties: polynomial Response Surface approximation and Monte Carlo simulations

G. Milani

*DIS, Dipartimento di Ingegneria Strutturale, Politecnico di Milano,
Piazza Leonardo da Vinci 32, 20133 Milan, Italy*

D. Benasciutti[†]

*DIEGM, Dipartimento di Ingegneria Elettrica Gestionale Meccanica, University of Udine,
Via delle Scienze 208, 33100 Udine, Italy*

(Received September 3, 2008, Accepted November 16, 2009)

Abstract. The uncertainty often observed in experimental strengths of masonry constituents makes critical the selection of the appropriate inputs in finite element analysis of complex masonry buildings, as well as requires modelling the building ultimate load as a random variable. On the other hand, the utilization of expensive Monte Carlo simulations to estimate collapse load probability distributions may become computationally impractical when a single analysis of a complex building requires hours of computer calculations. To reduce the computational cost of Monte Carlo simulations, direct computer calculations can be replaced with inexpensive Response Surface (RS) models. This work investigates the use of RS models in Monte Carlo analysis of complex masonry buildings with random input parameters. The accuracy of the estimated RS models, as well as the good estimations of the collapse load cumulative distributions obtained via polynomial RS models, show how the proposed approach could be a useful tool in problems of technical interest.

Keywords: Monte Carlo method; masonry; limit analysis; homogenization; polynomial Response Surface; Latin Hypercube method; collapse load probability distribution.

1. Introduction

The structural analysis of masonry buildings under seismic actions is generally very complex and usually requires complicate nonlinear analyses, performed nowadays with finite elements (FE) methods.

The collapse load of a given building is clearly a function of the geometry, of the external actions, of the materials properties and finally of the environmental conditions (humidity, temperature). In the technical literature, many different methods based on FE simulations can be found for the

[†] Assistant Professor, Corresponding author, E-mail: denis.benasciutti@uniud.it

evaluation of the ultimate loads of engineering structures (see for instance Milani *et al.* 2006a, 2006c, 2007a, Olsen 2001, Sloan and Kleeman 1995). A suitable way, which requires a relatively low computational cost, is the use of limit analysis theorems in combination with finite elements. Such approach is able to give important information at failure, such as for instance collapse loads, failure mechanisms and, at least on critical sections, the stress distribution. The hypotheses at the base of the method are statically applied loads, infinite ductility and associated flow rules for the constituent materials. These hypotheses yield well for steel structures (see Olsen 2001), but it has been shown that quite reliable results can be obtained also for concrete (Olsen 1999) and masonry (Sutcliffe *et al.* 2001, Milani *et al.* 2006a) materials that, as well known, exhibit a finite ductility. Nevertheless, an analysis at collapse for masonry structures remains a very difficult task, both from a theoretical and numerical point of view, essentially because brickwork is constituted by an assemblage of bricks between which thin mortar joints are laid. At present, the three approaches most utilized in practice to tackle engineering problems involving the study of masonry structures rely on micro-modelling (Bicanic *et al.* 2003, Lofti and Shing 1994), macro-modeling (Lourenço *et al.* 1997) and homogenization (Sejnoha *et al.* 2008, Milani *et al.* 2006b). An alternative technically meaningful methodology is finally represented by the so-called macro-elements approach presented, for instance, in Magenes and Calvi 1997.

While micro-modeling is limited to small structures (Milani *et al.* 2007b), since a separate modeling of bricks and joints is required in the framework of finite elements, in macro-modeling the heterogeneous material is substituted with a macroscopic homogeneous fictitious one, obtained essentially from experimental data fitting. Despite the fact that macro-modeling is suitable for large scale structures, it requires a difficult calibration of its mechanical properties, usually obtained by means of costly experimental campaigns (Lourenço 1999).

In light of these considerations, homogenization theory seems particularly attractive, since it is able to reproduce macroscopic masonry behavior at failure requiring only the knowledge of mechanical properties of the constitutive materials (always available with low cost), once that a suitable repetitive unitary cell is found.

As a result, in the framework of homogenization and limit analysis, for a fixed building geometry and for a given set of applied external actions, the building collapse load y resulting from FE calculations will only depend on the input materials properties (bricks and mortar), as formalized by the mathematical model

$$y = h(\mathbf{x}) \quad (1)$$

where vector $\mathbf{x} = (x_1, x_2, \dots, x_m)$ collects all the relevant input material parameters (e.g., cohesion, friction angle, cut-off stress, joints and bricks compressive strength, etc.). Function $h(-)$, even though highly non-linear, is strictly deterministic, i.e., replicated calculations from running the same input materials parameters will give the same output collapse load.

The relevant input strength properties $\mathbf{x} = (x_1, x_2, \dots, x_m)$ are generally characterized by an intrinsic statistical variability -often classified as stochastic uncertainty (Helton 1997, Helton and Burmaster 1996, Paté-Cornell 1996, Winkler 1996, Hoffman and Hammonds 1994, Helton 1994, Apostolakis 1990, Haan 1989, Parry and Winter 1981)- since strength varies among nominally identical test specimens, independently of the sample size used.

On the other hand, the material strength properties of single masonry constituents (e.g., mortar, brick) are usually determined in civil engineering through very few experimental tests and often show a very large scatter (Brenchich and Gambarotta 2005, Vermeltoort 2006, van der Pluijm 1999).

Therefore, the lack of knowledge from insufficient experimentation obviously corresponds to an epistemic uncertainty in the estimation of distributions parameters.

As a consequence, the selection of appropriate values to use in FE simulations could become a critical task. For instance, experimental data are quite often so spread, that simply using mean values could give unsafe results. In addition, the variability in materials strength properties also induces an uncertainty in the resultant collapse load; clearly, the use of mean values to define the building resistance could be greatly unsafe. Even the so called characteristic value approach, often used in building practice, could not be a reliable alternative. In fact, despite such an approach refers to a small occurrence probability (usually 5%) of a Gaussian distribution to safely define a single input strength value (the Gaussian distribution being estimated from a very small experimental data set, e.g., three specimens of masonry compressive strength according to the Italian code), it only determines a unique ultimate building strength, with no information on the entire probability distribution and collapse probabilities.

As a consequence, a much more reliable approach would require using a probabilistic analysis to estimate the probability distribution of the building limit load (assigned the probability distributions of the input strength properties of single masonry constituents) and then calculating failure probabilities and safety levels.

However, explicit determination of the collapse load probability distribution needs explicit knowledge of function $h(-)$, which unfortunately is rarely known in a closed-form.

A possible alternative is to use an approximate probabilistic analysis based on extensive Monte Carlo (MC) simulations, in which sampling-based techniques are used to study how uncertainty propagates from random input parameters to the calculated analysis results, by repetitively selecting values for the random input variables and then calculating the corresponding analysis outputs, see Fig. 1. The complete set of calculated building collapse loads constitutes an observed sample, which can be used to estimate the collapse load probability distribution. Since in MC method the input values are chosen at random from their own domains of definition, the sampled values, as well as the calculated output, are more likely to occur in regions associated to high probabilities, usually around the mean of the distribution. Hence, large sample sizes (i.e., many simulations runs) are needed to assure a reasonable coverage of the range of each input variable (and of the calculated analysis output), as well as to achieve a sufficient statistical convergence of the estimated output probability distribution.

Considering that, despite computational improvements, a single FE limit analysis of a complex building could take many hours of calculations (see Yu and Tin-Loi 2006), the large sample sizes used by extensive MC simulations become prohibitive for practical applications.

To alleviate the overall computational cost, a possibility is to replace the MC method with improved sampling-based techniques, which guarantee the same statistical convergence with smaller sample sizes. As an example, in importance (or stratified) sampling the sample space is properly divided into non-overlapping sub-regions of pre-assigned probability, to assure a better coverage of input domain while allowing as lower sample sizes as possible, although the correct identification of sub-regions may result a complex task (Glynn and Iglehart 1989, Melchers 1990, Goyal *et al.* 1992, Shahabuddin 1994, Heidelberger 1995, Owen and Zhou 2000, Nicola *et al.* 2001). An approach which may be viewed as a compromise procedure between simple random sampling with large samples and importance sampling is Latin Hypercube (LH) method, which adopts a random sampling for each input variable over sub-regions of equal probability. Due to its advantages, in the last decades the LH method has received an increasing attention in many different research areas

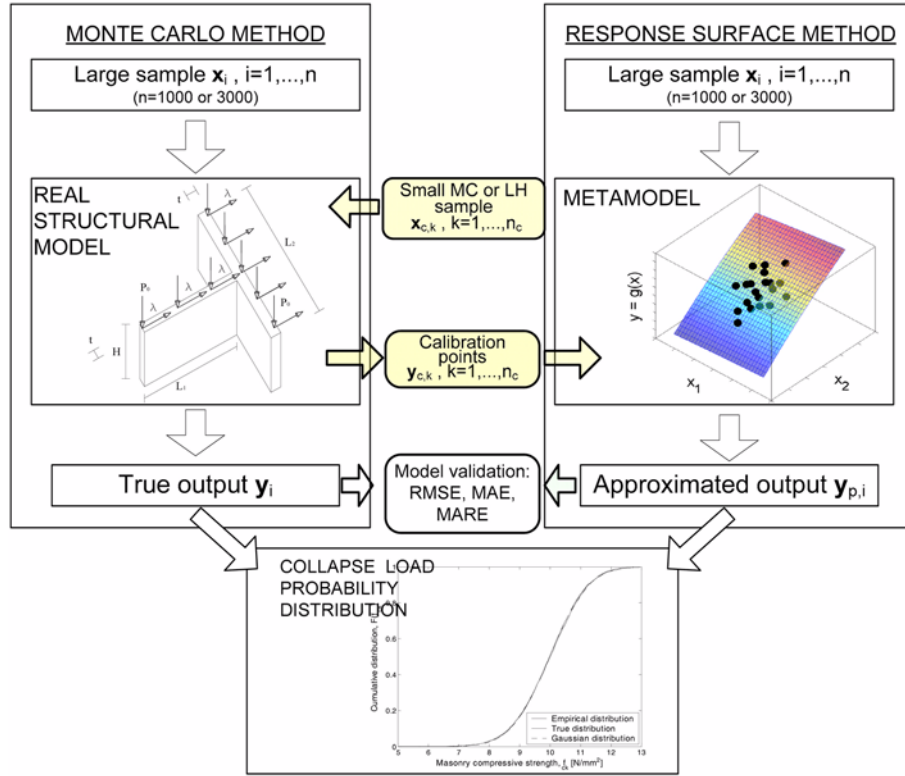


Fig. 1 Schematic representation of extensive Monte Carlo simulations (via direct computer calculations or via RS model) used to estimate the collapse load probability distribution. Construction and validation of the polynomial RS model is also shown

and applications, where the use of large samples is not computationally practicable (Helton and Davis 2003, Hradil *et al.* 2001, McKay *et al.* 1979). However, even though the LH method can help in reducing the total number of simulation runs required, in some applications the overall simulation time could still remain unacceptably high.

A completely different approach which can drastically reduce the total computation time is to adopt the so-called response surface (RS) technique to construct a surrogate model (or metamodel), that can be used as inexpensive mathematical approximation of the actual, yet time-consuming, computer simulation (Giunta and Watson 1998, Jin *et al.* 2001, Simpson *et al.* 2001, 2002, Swiler *et al.* 2006). More precisely, function $h(-)$ introduced in Eq. (1), formalizing the actual FE input/output relationship of a FE limit analysis, is replaced by an approximation $\hat{h}(-)$, which is calibrated on few observed outputs, resulting from running computer calculations on a small set of optimally selected design inputs, see Fig. 1.

Assumed that the overall approximation error is sufficiently small and technically acceptable, the decisive advantage of RS techniques is that the sample sizes required for an accurate calibration are significantly lower (e.g., two order of magnitude) than those used in extensive MC simulations.

Once the RS model has been calibrated, it can be used as a proxy of direct computer calculations in extensive MC simulations, which are used to generate large sets analysis outputs to estimate the output probability distribution.

Different RS models exist, which differ in respect to their relative accuracy and complexity. Even though many studies have investigated what combination of design scheme and RS technique would give the best accuracy, no general rules were found for all engineering problems (Giunta and Watson 1998, Jin *et al.* 2001, Simpson *et al.* 2001, 2002, Swiler *et al.* 2006). On the other hand, other aspects than accuracy were indicated as equally important: robustness (accuracy and stability through different types of problems), efficiency (computational effort required in metamodel calibration), transparency (existence of explicit relationships between inputs and outputs) and conceptual simplicity (easiness of implementation). As an example, the classical polynomial RS approximation, which was indicated as the optimal choice due to its great simplicity and possible fairly good accuracy (Jin *et al.* 2001), has been used (Neves *et al.* 2006, Pendola *et al.* 2000) for several technical applications in the framework of mildly nonlinear problems, demonstrating its robustness and accuracy. On the other hand, in problems with a high nonlinear behavior the response surface approximation based on nonparametric regression may be particularly effective (Storlie and Helton 2008a, b, Storlie *et al.* 2009).

With the aim of investigating the potentiality of polynomial RS models in replacing actual computer simulations in the homogenized limit analysis of complex masonry buildings with random input parameters, this work will attempt:

- to investigate the accuracy and efficiency of polynomial RS models as inexpensive replacement of direct computer simulations;
- to study the correlation between RS accuracy and design scheme, by referring to the MC and the LH techniques for generating input points for RS fitting;
- to evaluate the accuracy of the estimated output probability distribution when polynomial RS models are used in place of direct computer calculations in extensive MC simulations.

The utilization of limit analysis in combination with RS approximation seems particularly adequate, since the response of limit analysis is smooth with respect to variation of material parameters. Obviously, the extension of this statement to experimentally observed data is, in principle, not possible because of the practical impossibility to perform extensive experimental MC tests on real scale masonry structures.

In the present work, numerical simulations concerning three examples of relevant technical interest (i.e., a masonry compressive behavior, an in- and out-of-plane loaded masonry wall and a shear panel) are presented.

At a first attempt, a quadratic polynomial RS model is constructed on a small set of observed analysis outputs, resulting from running computer simulations on a small set of input points (at most 20 or 30), generated by either the MC method or the LH technique.

The estimated polynomial RS model is then used in place of direct computer calculations in extensive MC simulations with large sample sizes, used to assess the collapse load probability distribution.

A comparison between the probability distribution estimated via RS model and the one obtained by direct computer calculations is presented.

The same large MC samples are also used as validation points to compare the fitting performance of RS models constructed from MC or LH design points.

The presented results show how the use of polynomial RS with MC simulations can drastically reduce the overall computation time, providing acceptable levels of accuracy and assuring also quite good estimates of the collapse load probability distribution.

2. Probabilistic analysis with homogenized limit analysis and polynomial RS models

2.1 Masonry homogenized failure surfaces

Failure loads of complex 3D masonry structures can be obtained with a relatively low computational cost by means of a recently presented FE limit analysis approach (Milani *et al.* 2006b), in which masonry failure surface is obtained through a micro-mechanical model which bases on homogenization theory applied in the rigid-plastic case.

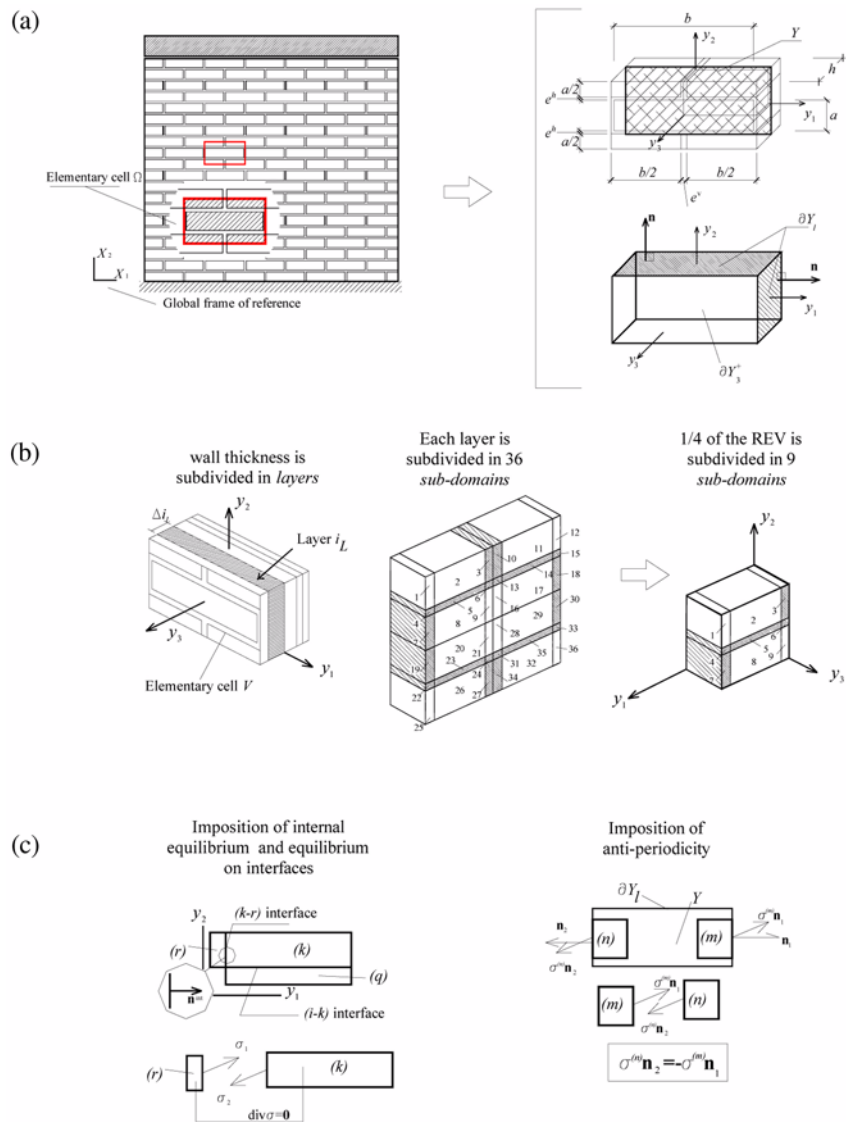


Fig. 2 Proposed micro-mechanical model (a) elementary cell, (b) subdivision in layers along thickness and subdivision of each layer in sub-domains, (c) imposition of internal equilibrium, equilibrium on interfaces and anti-periodicity

A detailed description of the equilibrated micro-mechanical model adopted is reported in (Milani *et al.* 2006a, b, c, 2007a) and the reader is referred there for an exhaustive discussion. In this section, only the basic idea of the model proposed is recalled in order to show how FE homogenized limit analysis Monte Carlo simulations have been performed at a structural level.

In Fig. 2(a), a masonry wall Ω constituted by a periodic arrangement of bricks and mortar disposed in running bond texture is reported. Following the general procedure proposed in (Suquet 1983), homogenization techniques combined with limit analysis can be used for the evaluation of masonry homogenized strength domain S^{hom} for combined in- and out-of-plane loads. In the framework of the lower bound limit analysis theorem (i.e., assuming associated flow rules for the constituent materials and imposing equilibrium equations and admissibility conditions), it can be shown that the frontier ∂ of S^{hom} is obtained solving the following linear programming problem (see also Fig. 2)

$$\partial S^{\text{hom}} = \left\{ \max(\mathbf{M}, \mathbf{N}) \right\} \left\{ \begin{array}{l} \mathbf{N} = \frac{1}{|Y|} \int_{Y \times \left[-\frac{h}{2}, \frac{h}{2}\right]} \boldsymbol{\sigma} dV \quad (a) \\ \mathbf{M} = \frac{1}{|Y|} \int_{Y \times \left[-\frac{h}{2}, \frac{h}{2}\right]} y_3 \boldsymbol{\sigma} dV \quad (b) \\ \text{div } \boldsymbol{\sigma} = \mathbf{0} \quad (c) \\ \llbracket \boldsymbol{\sigma} \rrbracket \mathbf{n}^{\text{int}} = \mathbf{0} \quad (d) \\ \boldsymbol{\sigma} \mathbf{n} \text{ anti-periodic on } \partial Y_l \quad (e) \\ \boldsymbol{\sigma}(\mathbf{y}) \in S^m \quad \forall \mathbf{y} \in Y^m; \quad \boldsymbol{\sigma}(\mathbf{y}) \in S^b \quad \forall \mathbf{y} \in Y^b \quad (f) \end{array} \right. \quad (2)$$

In Eq. (2) the following symbols have been used:

- \mathbf{N} and \mathbf{M} , which represent macroscopic in-plane (membrane forces) and out-of-plane (bending moments and torsion) tensors;
- $\boldsymbol{\sigma}$, which is the projection of the local stress tensor along directions y_1 and y_2 , see Fig. 2;
- \mathbf{n} , the outward unit vector orthogonal to ∂Y_l surface, Fig. 2(a);
- ∂Y_l , which is the internal boundary of the elementary cell, Fig. 2(a);
- $\llbracket \boldsymbol{\sigma} \rrbracket$, representing the jump of micro-stresses across any discontinuity surface of normal \mathbf{n}^{int} , Fig. 2(c);
- S^m and S^b , denoting respectively the strength domains of mortar and bricks;
- Y , which is the cross section of the 3D elementary cell with $y_3 = 0$ (see Fig. 2), $|Y|$ is its area, V is the elementary cell volume, h represents the wall thickness and $\mathbf{y} = (y_1 \ y_2 \ y_3)$ is the position of a point in the local frame of reference.

As shown in Fig. 2(b), in the model the unit cell is subdivided into a fixed number of layers along its thickness. For each layer out-of-plane components σ_{i3} ($i = 1, 2, 3$) of the micro-stress tensor $\boldsymbol{\sigma}$ are set to zero (i.e., a typical plane stress condition for each layer is adopted), so that only in-plane components σ_{ij} ($i, j = 1, 2$) are considered active. Furthermore, σ_{ij} ($i, j = 1, 2$) are kept constant along the thickness Δ_{i_l} of each layer, i.e., in each layer $\sigma_{ij} = \sigma_{ij}(y_1, y_2)$. For each layer, each fourth of the representative volume element is sub-divided into nine geometrical elementary entities (sub-domains), so that the entire elementary cell is sub-divided into 36 sub-domains (see Milani *et al.*

2006b and Fig. 2(b) for further details).

For each sub-domain k and layer i_L , polynomial distributions of degree (m) in the variables (y_1, y_2) are a priori assumed for the stress components. Since stresses are polynomial expressions, the generic ij th component can be written as follows

$$\sigma_{ij}^{(k, i_L)} = \mathbf{X}(\mathbf{y}) \mathbf{S}_{ij}^{(k, i_L)T} \quad \mathbf{y} \in Y^{(k, i_L)} \quad (3)$$

Where, $\mathbf{X}(\mathbf{y}) = [1 \ y_1 \ y_2 \ y_1^2 \ y_1 y_2 \ y_2^2 \ \dots]$, $Y^{(k, i_L)}$ represents the k th sub-domain of layer (i_L) and $\mathbf{S}_{ij}^{(k, i_L)} = [S_{ij}^{(k, i_L)(1)} \ S_{ij}^{(k, i_L)(2)} \ S_{ij}^{(k, i_L)(3)} \ S_{ij}^{(k, i_L)(4)} \ S_{ij}^{(k, i_L)(5)} \ S_{ij}^{(k, i_L)(6)} \ \dots]$ is a vector representing the unknown stress parameters of sub-domain k of layer i_L .

The imposition of equilibrium inside each sub-domain, the continuity of the stress vector on interfaces and the anti-periodicity of $\boldsymbol{\sigma} \mathbf{n}$ permit a strong reduction in the number of independent stress parameters (see Milani *et al.* 2006b for further details), allowing to write the stress vector $\tilde{\boldsymbol{\sigma}}^{(k, i_L)}$ of layer i_L inside each sub-domain as $\tilde{\boldsymbol{\sigma}}^{(k, i_L)} = \tilde{\mathbf{X}}^{(k, i_L)}(\mathbf{y}) \tilde{\mathbf{S}}^{(i_L)}$ where $\tilde{\mathbf{S}}^{(i_L)}$ is the vector of linearly independent unknown stress parameters of layer i_L , k is a sub-domain and $\tilde{\mathbf{X}}^{(k, i_L)}$ is a $3 \times n_s$ matrix, which depends only on the geometry of the sub-domain (n_s is the length of vector $\tilde{\mathbf{S}}^{(i_L)}$).

Once that an equilibrated polynomial field in each layer is obtained (here fourth-order polynomials are used), the proposed in- and out-of-plane model requires a subdivision of the wall thickness into n_L layers (Fig. 2(b)), with a constant thickness $\Delta_{i_L} = h/n_L$. This allows to derive the following simple non-linear optimization problem

$$\partial S^{\text{hom}} \equiv \left\{ \begin{array}{l} \text{such that} \\ \left\{ \begin{array}{ll} \max(\lambda) & \\ \tilde{\mathbf{N}} = \int_{k, i_L} \tilde{\boldsymbol{\sigma}}^{(k, i_L)} dV & (a) \\ \tilde{\mathbf{M}} = \int_{k, i_L} y_3 \tilde{\boldsymbol{\sigma}}^{(k, i_L)} dV & (b) \\ \boldsymbol{\Sigma} = [\tilde{\mathbf{N}} \ \tilde{\mathbf{M}}] = \lambda \mathbf{n}_{\boldsymbol{\Sigma}} & (c) \\ \tilde{\boldsymbol{\sigma}}^{(k, i_L)} = \tilde{\mathbf{X}}^{(k, i_L)}(\mathbf{y}) \tilde{\mathbf{S}}^{(i_L)} & (d) \\ \tilde{\boldsymbol{\sigma}}^{(k, i_L)} \in S^{(k, i_L)} & (e) \\ k = 1, \dots, \text{ number of sub-domains} & (f) \\ i_L = 1, \dots, \text{ number of layers} & (g) \end{array} \right. \end{array} \right. \quad (4)$$

In Eq. (4) λ represents the so-called load multiplier, $S^{(k, i_L)}$ denotes the non-linear strength domain of the constituent material (mortar or brick) corresponding to the k th sub-domain and i_L th layer. As a rule, λ is an ultimate moment, an ultimate membrane action or a combination of moments and membrane actions. In order to recover ∂S^{hom} surface point by point, a fixed direction $\mathbf{n}_{\boldsymbol{\Sigma}}$ in the six dimensional space of membrane actions ($\tilde{\mathbf{N}} = [N_{xx} \ N_{xy} \ N_{yy}]$) and bending + torsion moments ($\tilde{\mathbf{M}} = [M_{xx} \ M_{xy} \ M_{yy}]$) is chosen. For each $\mathbf{n}_{\boldsymbol{\Sigma}}$, a failure load λ at a cell level is computed. The knowledge of $\mathbf{n}_{\boldsymbol{\Sigma}}$ and λ permits to find a point of the masonry failure surface in six dimensions. Changing the direction $\mathbf{n}_{\boldsymbol{\Sigma}}$, a new λ is calculated from the optimization problem, hence a new point

of the failure surface is collected. In this manner, repeating the procedure for a suitable number of different directions, several points of ∂S^{hom} can be calculated. With the hypotheses assumed in (Milani *et al.* 2006b) ∂S^{hom} results convex. Therefore, a final Delaunay tessellation permits to find a lower bound linear approximation of ∂S^{hom} .

A linearization with 80 planes of such failure surface is implemented in the FE limit analysis code described in the following section, for performing the upper bound homogenized limit analyses presented in this paper.

Of course, the failure surface obtained with the homogenization procedure presented above depends on both mechanical properties assumed for joints and bricks; therefore, also the collapse load of the structures considered in Example 2 and 3 of this paper indirectly depends on both bricks and mortar mechanical properties. Finally, it is worth noting that, in principle, also fracture energy of constituent materials should be ideally considered as a random variable (see van der Pluijm 1999), although in limit analysis fracture energy effect is disregarded.

2.2 3D kinematic FE limit analysis

The upper bound approach developed in this paper is fully described in (Milani *et al.* 2007a) and the reader is referred there for a detailed description of the numerical model. Here, only the bases of the procedure proposed are reported. The formulation uses three noded triangular elements with linear interpolation of the velocity field inside each element, so that three velocity unknowns per node i , say w_{xx}^i , w_{yy}^i and w_{zz}^i (respectively 2 in-plane velocities and 1 out-of-plane velocity, see Fig. 3(a)) are introduced for each element E , meaning that the velocity field is linear inside an element.

A possible jump of velocities on interfaces between adjoining elements is supposed to occur, with linear interpolation of the jump along the interface. The introduction of a jump of displacements is useful to obtain reliable collapse loads for friction materials (see Sloan and Kleeman 1995). In this framework, for each interface between coplanar adjacent elements, four additional unknowns are

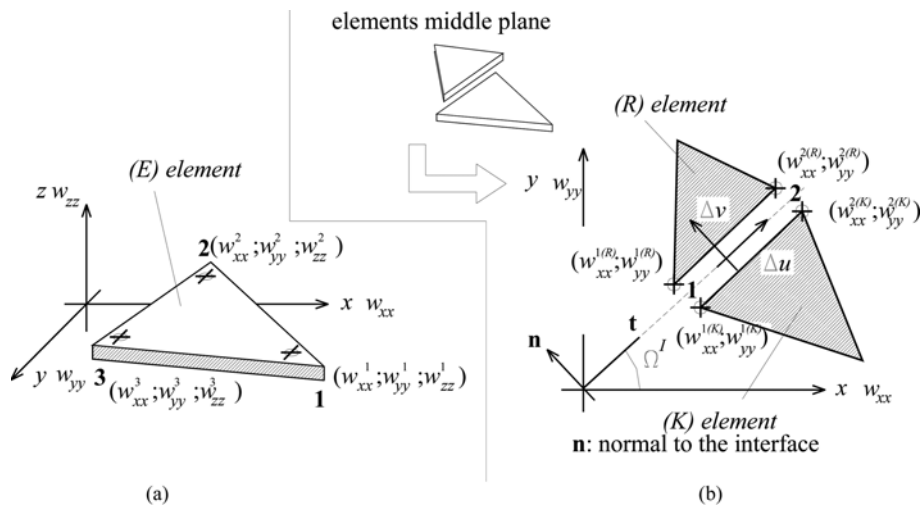


Fig. 3 (a) Triangular plate and shell element used for the upper bound FE limit analysis, (b) discontinuity of the in-plane velocity field

introduced ($\Delta \mathbf{u}^I = [\Delta v_1 \ \Delta u_1 \ \Delta v_2 \ \Delta u_2]^T$), representing the normal (Δv_1) and tangential (Δu_i) jumps of velocities (with respect to the discontinuity direction) evaluated on nodes $i = 1$ and $i = 2$ of the interface (see Fig. 3(b)). For any pair of nodes on the interface between two adjacent and coplanar triangles R and K , the tangential and normal velocity jumps can be written in terms of the Cartesian nodal velocities of elements R - K (see Fig. 3 for details), so that a system of four linear equations in the form $\mathbf{A}_{11}^{eq} \mathbf{w}^R + \mathbf{A}_{12}^{eq} \mathbf{w}^K + \mathbf{A}_{13}^{eq} \Delta \mathbf{u}^I = \mathbf{0}$ can be written, being \mathbf{w}^R and \mathbf{w}^K the 9×1 vectors that collect velocities of elements R and K respectively and \mathbf{A}_{1j}^{eq} $j = 1, 2, 3$ matrices which depend only on the interface orientation Ω^I (Fig. 3).

Since velocities interpolation is kept linear inside each triangular element, only three equality constrains representing the plastic flow in continuum (obeying an associated flow rule) are introduced for each element in the form $\dot{\boldsymbol{\epsilon}}_{pl}^E = \dot{\lambda}^E \partial S^{\text{hom}} / \partial \boldsymbol{\Sigma}$, where $\dot{\boldsymbol{\epsilon}}_{pl}^E$ is the plastic strain rate vector of element E , $\dot{\lambda}^E \geq 0$ is the plastic multiplier, S^{hom} is the homogenized (non) linear failure surface of masonry in the six dimensional space of membrane N_{11}, N_{12}, N_{22} and bending M_{11}, M_{12}, M_{22} actions, i.e., $\boldsymbol{\Sigma} = (N_{11}, N_{12}, N_{22}, M_{11}, M_{12}, M_{22})$.

For each element, plastic flow in continuum may be written in the form $\mathbf{A}_{11}^{eq} \mathbf{w}^E + \mathbf{A}_{12}^{eq} \dot{\boldsymbol{\lambda}}^E = \mathbf{0}$, where \mathbf{w}^E is the vector of element velocities and $\dot{\boldsymbol{\lambda}}^E$ is a $m \times 1$ vector of plastic multiplier rates, one for each plane of the linearized failure surface.

Denoting with $\mathbf{w}_{zz,E} = [w_{zz}^{i(E)} \ w_{zz}^{j(E)} \ w_{zz}^{k(E)}]^T$ the element E out-of-plane nodal velocities and with $\dot{\boldsymbol{\theta}}_E = [\dot{\theta}_i^E \ \dot{\theta}_j^E \ \dot{\theta}_k^E]^T$ the side normal rotation rates, it is possible to show that $\dot{\boldsymbol{\theta}}_E$ and $\mathbf{w}_{zz,E}$ are linked by the compatibility equation (Fig. 4) $\dot{\boldsymbol{\theta}}_E = \mathbf{B}_E \mathbf{w}_{zz,E}$, where \mathbf{B}_E is a 3×3 matrix that depends only on the geometry of element E .

The total internal power dissipated P^{in} is constituted by the power dissipated in continuum, P_E^{in} , and the power dissipated on interfaces, P_I^{in} . It is interesting to note that out-of-plane plastic dissipation occurs only along each interface I between two adjacent triangles R and K or on a boundary side B of an element Q (see Fig. 4). Therefore P_E^{in} can be evaluated for each triangle E of area A_E taking into account only in-plane actions.

Let us assume that a linear approximation (with m hyper-planes) of masonry failure surface in the form $S^{\text{hom}} \equiv \mathbf{A}^{in} \boldsymbol{\Sigma} \leq \mathbf{b}^{in}$ is at disposal solving, as already discussed in the previous Section, a number of linear programming problems (4). Here, \mathbf{A}^{in} is a $m \times 6$ matrix of coefficients of each hyper-plane and \mathbf{b}^{in} is a $m \times 1$ vector of the right hand sides of the linear approximation.

As the homogenized (linearized) failure surface is constituted by m hyper-planes of equation

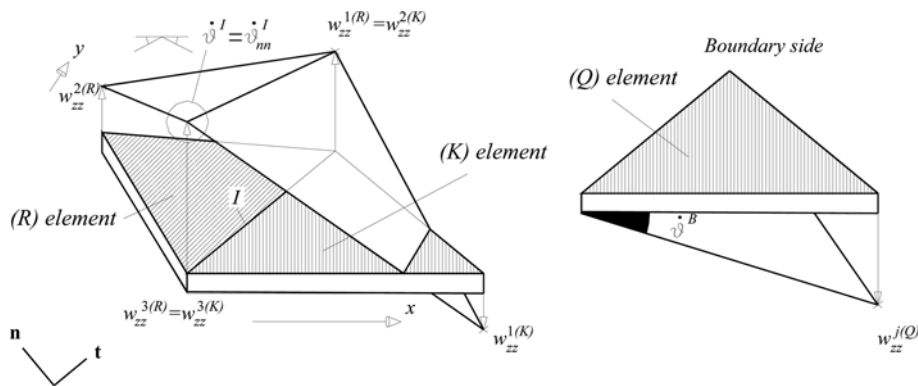


Fig. 4 Rotation along an interface between adjacent triangles or in correspondence of a boundary side

$A_{xx}^q N_{xx} + A_{yy}^q N_{yy} + A_{xy}^q N_{xy} + B_{xx}^q M_{xx} + B_{yy}^q M_{yy} + B_{xy}^q M_{xy} = C_E^q$, with $1 \leq q \leq m$, an estimation of P_E^{in} can be easily obtained as $P_E^{in} = A_E \sum_{q=1}^m C_E^q \dot{\lambda}_E^{(q)}$ with curvature rate tensor equal to zero, being $\dot{\lambda}_E^{(q)}$ the plastic

multiplier rate of the triangle E associated to the q th hyper-plane of the linearized failure surface.

On the other hand, for an interface I between adjoining elements of length Γ and orientation Ω^I , a rotation operator is applied to the linearized homogenized admissible domain frontier in order to obtain with a limited computational effort m equations (one for each hyper-plane) in the form $A_{tt}^q N_{tt} + A_{nn}^q N_{nn} + A_{tn}^q N_{tn} + B_{tt}^q M_{tt} + B_{nn}^q M_{nn} + B_{tn}^q M_{tn} = C_I^q$ representing $\partial \tilde{S}^{\text{hom}}$ in the $\mathbf{n}-\mathbf{t}$ interface frame of reference, defined in Fig. 3.

In this way, the power dissipated P_I^{in} along an interface I can be easily estimated as reported in (Krabbenhoft *et al.* 2005) and the reader is referred there for a detailed discussion of the kinematic hypotheses adopted for the evaluation of P_I^{in} .

After some assemblage operations (see for instance Olsen 2001, Sloan and Kleeman 1995, Krabbenhoft *et al.* 2005), the following linear programming problem is obtained, where the objective function is the total internal power dissipated

$$\min \left\{ \sum_{I=1}^{n^I} P_I^{in} + \sum_{E=1}^{n^E} P_E^{in} - \mathbf{P}_0^T \mathbf{w} \right\} \text{ such that } \begin{cases} \mathbf{A}^{eq} \mathbf{U} = \mathbf{b}^{eq} \\ \dot{\lambda}^{I,ass} \geq \mathbf{0} \quad \dot{\lambda}^{E,ass} \geq \mathbf{0} \\ \dot{\theta}^{ass} = \dot{\theta}^+ - \dot{\theta}^- \\ \dot{\theta}^+ \geq 0 \quad \dot{\theta}^- \geq 0 \end{cases} \quad (5)$$

In Eq. (5) the following symbols are used:

- \mathbf{U} is the vector of global unknowns and collects the vector of assembled nodal velocities (\mathbf{w}), the vector of assembled element plastic multiplier rates ($\dot{\lambda}^{E,ass}$), the vector of assembled jump of velocities on interfaces ($\Delta \mathbf{u}^{I,ass}$), the vector of assembled interface plastic multiplier rates ($\dot{\lambda}^{I,ass}$) and the vector of interface and boundary out-of-plane rotation rates $\dot{\theta}^{ass}$.
- \mathbf{A}^{eq} is the overall constraints matrix and collects normalization conditions, velocity boundary conditions, relations between velocity jumps on interfaces and elements velocities, constraints for plastic flow in velocity discontinuities and constraints for plastic flow in continuum.
- n^E and n^I are the total number of elements and interfaces, respectively.
- \mathbf{P}_0 is the vector of (equivalent nodal) permanent loads.

2.3 Polynomial Response Surface (RS) modelling

Given the vector \mathbf{x}_i of analysis inputs for the i th computer simulation, a quadratic polynomial RS model has the form

$$y_{p,i} = c_0 + \sum_{q=1}^m c_q x_{i,q} + \sum_{q=1}^m \sum_{r=q}^m c_{qr} x_{i,q} x_{i,r} \quad (6)$$

where m is the total number of input variables (i.e., random material properties), $x_{i,q}$ is the value of the q th input variable for the i th computer run and c_q are (unknown) coefficients.

Given n independent observed analyses outputs y_i , $i = 1, \dots, n$, the estimation problem can be formulated in compact matrix notation as

$$\mathbf{y} \approx \mathbf{X}\hat{\mathbf{c}} \quad (7)$$

where \mathbf{y} is the vector of observed outputs, \mathbf{X} is the so called design matrix, while the unique least-squares estimator of the unknown coefficients is

$$\hat{\mathbf{c}} = (\mathbf{X}^T \mathbf{X})^{-1} \mathbf{X}^T \mathbf{y} \quad (8)$$

A RS model is fitted on a set $y_{c,k}$, $k = 1, \dots, n_c$ of observed analysis outputs, derived from computer calculations on a set of optimally selected values $\mathbf{x}_{c,k}$ for the relevant input variables. Different design of experiments strategies can be used to sample the input variables for RS fitting (Giunta *et al.* 2003).

Several studies in the literature, in trying to discover what design of experiment would provide the best accuracy, found that no method has been recognized as the best one (Simpson *et al.* 2001, 2002) and one should always refer to the specific problem under study (Simpson *et al.* 2002, Swiler *et al.* 2006), although according to Simpson *et al.* (2001) the basic requirement for an experimental design in deterministic computer analyses is space filling.

In the present work, the input design points are generated by two different sampling schemes: classical MC method and the LH technique, the latter being considered for its relative simplicity with respect to other existing techniques, and because it provides a better space filling compared to the MC method.

2.4 Experimental design: Monte Carlo and Latin Hypercube method

In the classical MC method, the input design random variables are selected at random from their domains of definition, hence the sampled values have more probability to occur in regions with higher probabilities (e.g., close to the mean value of the distribution).

To assure a more uniform sampling from the interval of each random variable the LH technique has been proposed as an improvement to the classical MC method (Helton and Davis 2003, McKay *et al.* 1979). In the LH method, to obtain a sample of size n_c by m input random variables $\mathbf{x} = (x_1, x_2, \dots, x_m)$, we first divide the definition domain of each variable in n_c disjoint intervals of equal probability, according to the corresponding probability distribution of each variable. Then, we extract a sample value from each interval, leading to a set of n_c sampled values for each variable. Compared to the classical MC method, the LH design assures that each of the input random variables has all portions of its range represented, thus providing a more uniform sampling of the input design space. Finally, the n_c samples for vector \mathbf{x} are obtained by combining all values previously sampled according to n_c random permutations. Special techniques are used to impose desired correlations among several variables, see Refs. (Helton and Davis 2003, Florian 1992, Huntington and Lyrintzis 1998).

2.5 Validation of fitted RS model

To quantify the prediction accuracy of an estimated RS model we calculate at n specified validation points the difference between the true analysis output y_i from a direct computer simulation and the value $y_{p,i}$ predicted by the polynomial RS model. Following some existing references (Simpson *et al.* 2002, Swiler *et al.* 2006, Ramu *et al.* 2007), we refer to the Root Mean Square Error (RMSE)

$$RMSE = \sqrt{\frac{1}{n} \sum_{i=1}^n (y_i - y_{p,i})^2} \quad (9)$$

to the Mean Absolute Error (MAE)

$$MAE = \frac{1}{n} \sum_{i=1}^n \left| \frac{y_i - y_{p,i}}{y_i} \right| \quad (10)$$

and to the Maximum Absolute Relative Error (MARE)

$$MARE = \max \left(\left| \frac{y_i - y_{p,i}}{y_i} \right|_{i=1, \dots, n} \right) \quad (11)$$

Note that while RMSE and MAE provide an average measure of the overall and local prediction accuracy, respectively, MARE quantifies the absolute worst relative prediction error.

In order to capture the trend of the prediction error as a function of the observed output values y_i , in addition to the errors introduced above we also consider the percentage relative error

$$err_i(\%) = 100 \cdot \left(\frac{y_i - y_{p,i}}{y_i} \right) \quad (12)$$

For each fitted RS model a value of RMSE, MAE and MARE error metrics is obtained, as well as a set of percentage relative errors, which depend on the particular set of MC and LH calibration points used to construct the RS model, and also on the particular set of validation points considered. In fact, due to the random sampling technique adopted to generate calibration points, different MC or LH small replicated samples lead, in general, to different polynomial RS models (even with the same degree). On the other hand, the authors experienced that the use of MC and LH sampling performs better with respect to the use of a simple regular input grid, as a consequence of the over fitting polynomial approximation, see Giunta and Watson (1998). Hence, replicated samples are used to account for the variability in RS model generation, as well as in the considered set of validation points (see Iman 1981, Helton *et al.* 2005). More precisely, 10 replicated RS model from MC and LH calibration points and three independent large MC samples as validation points are considered.

3. Numerical simulations

Three examples of practical interest are examined to illustrate the use of polynomial RS models as a computationally inexpensive alternative to direct computer calculations in extensive MC simulations, used to estimate the collapse load probability distribution of masonry buildings having random material properties.

A common procedure is adopted in all examples. As a first step, a polynomial RS model is fitted on a small set of n_c observed collapse load values $y_{c,k}$, obtained from $\mathbf{x}_{c,k}$ input values sampled by either the MC method or the LH technique, see Fig. 1. As suggested in Jin *et al.* (2001), the number n_c of calibration points can be correlated to the number of input random variables; in our examples, n_c equals 20 for two input variables problems (Examples 1 and 2), 30 for three input variables problems (Example 3). Where needed, the independence among input random variables

for LH samples is imposed by the procedure described in Huntington and Lyrintzis (1998).

As a second step, the fitted RS model is used in place of direct computer simulations in extensive MC simulations with large sample sizes (1000 or 3000). The size of large MC samples was chosen as a necessary compromise between the high computational cost of all numerical simulations and the required accuracy in the estimate of the collapse load probability distribution, as well as considering 5% as a sufficient value for the failure probability in technical applications. On the

Table 1 Mean and standard deviation of the random input parameters used in the presented numerical examples. All the random input variables x_i are assumed as independent and normally distributed

	Example 1		Example 2		Example 3			
	Unit compressive strength ^a [N/mm ²]	Mortar compressive strength ^a [N/mm ²]	Cohesion ^b [N/mm ²]	Tangent of friction angle ^b [-]	Cohesion ^b [N/mm ²]	Tangent of friction angle ^b [-]	Auxiliary variable [-]	Mortar tensile strength ^c [N/mm ²]
	$x_1 = f_{cu}$	$x_2 = f_{cm}$	$x_1 = c$	$x_2 = \tan(\Phi)$	$x_1 = c$	$x_2 = \tan(\Phi)$	$x_3 = a$	$f_t = a \frac{c}{\tan(\Phi)}$
Mean value	19.91	14.72	0.1457	0.75	0.142	0.752	0.5	0.0948
Standard deviation	2.845	0.566	0.034	0.045	0.036	0.047	0.036	0.0258

^aEstimated from experimental data reported in (Brencich and Gambarotta 2005)

^bEstimated from experimental data reported in (van der Pluijm 1999)

^cMean and standard deviation for variable f_t are derived as in Appendix B, see Eq. (24)

Table 2 Theoretical mean and standard deviation (bold numbers) of the random input parameters (see Table 1) compared with those calculated on the three large MC samples

	Example 1		Example 2		Example 3		
	Unit compressive strength [N/mm ²]	Mortar compressive strength [N/mm ²]	Cohesion [N/mm ²]	Tangent of friction angle [-]	Cohesion [N/mm ²]	Tangent of friction angle [-]	Mortar tensile strength [N/mm ²]
MC sample	$x_1 = f_{cu}$	$x_2 = f_{cm}$	$x_1 = c$	$x_2 = \tan(\Phi)$	$x_1 = c$	$x_2 = \tan(\Phi)$	$f_t = a \frac{c}{\tan(\Phi)}$
Mean value	19.91	14.72	0.1457	0.75	0.142	0.752	0.0948
MC1	19.93	14.73	0.143	0.753	0.143	0.751	0.0954
MC2	19.93	14.72	0.143	0.752	0.140	0.754	0.0935
MC3	19.88	14.73	0.142	0.751	0.142	0.754	0.0948
Standard deviation	2.845	0.566	0.034	0.045	0.036	0.045	0.0258
MC1	2.902	0.568	0.036	0.048	0.036	0.048	0.0259
MC2	2.788	0.562	0.037	0.046	0.034	0.049	0.0246
MC3	2.919	0.569	0.036	0.048	0.035	0.047	0.0254

other hand, considering the large variability of input material properties due to usually scarce experimental tests, higher sample size would unnecessarily increase the overall computational cost, without improving the accuracy of the tail estimates of the collapse load probability distribution.

A summary of the theoretical mean and standard deviation for all input variables is given in Table 1; the good agreement with the mean and standard deviation calculated on each large MC sample, reported in Table 2, confirms the correctness of the sizes adopted for large MC samples.

In the third step, the n collapse load values y_i , $i = 1, \dots, n$ resulting from large MC simulations are used to compute the empirical cumulative distribution (Mood *et al.* 1974)

$$\hat{P}(y) = \sum_{i=1}^n u(y-y_i) \quad (13)$$

(where $u(x) = 1$ for $x > 0$ and zero elsewhere is an indicator function) which is an estimator of the collapse load probability distribution $P(y)$. Note that $\hat{P}(y)$ depends on the particular MC outputs y_i considered, hence it is affected by a statistical uncertainty. Replicated MC simulations are then used to estimate a mean empirical cumulative distribution (Helton and Davis 2003)

$$\bar{P}(y) = \frac{1}{n_r} \sum_{r=1}^{n_r} \hat{P}_r(y) \quad (14)$$

while a measure of the error in the estimate of $\bar{P}(y)$ is given by the standard deviation (Helton and Davis 2003)

$$\sigma_P = \left[\frac{1}{n_r(n_r-1)} \sum_{r=1}^{n_r} (\hat{P}_r(y) - \bar{P}(y))^2 \right]^{1/2} \quad (15)$$

n_r being the number of replicates (in our examples, $n_r = 3$). Despite a value $n_r = 3$ provides only a rough estimate of σ_P which however still remains of technical interest, larger values of n_r should be used to increase the accuracy of the estimated standard deviation.

Confidence-interval curves for $\bar{P}(y)$ can also be obtained. Specifically, the $1 - \alpha$ confidence interval is $\bar{P} \pm t_{1-\alpha/2} \sigma_P$, where $t_{1-\alpha/2}$ is the $1 - \alpha/2$ quantile of the t -distribution with $n_r - 1$ degrees of freedom (e.g., $t_{1-\alpha/2} = 2.262$ for $\alpha = 0.05$ and $n_r = 10$, see (Helton and Davis 2003, Mood *et al.* 1974).

Following the scheme of Fig. 1, direct computer calculations on the same large MC samples are also performed, in order to compare the collapse load empirical distribution obtained via direct simulations with the one calculated via fitted RS models.

As a final step, a comparison of the prediction accuracy of the RS models constructed on MC and LH calibration points is also examined in terms of the error measures introduced in Section 2.5. As done in Jin *et al.* (2001), the same three replicated large MC sets previously used to estimate the output probability distribution are used as validation points. To account for variability in RS model fitting, mean and variance of all error measures are calculated on 10 independently replicated MC-RS and LH-RS polynomials. Note that while the mean of the errors indicates the average accuracy of a RS model, the variance illustrates the variability (i.e., robustness) of the prediction accuracy (Jin *et al.* 2001).

3.1 Example 1: Masonry compressive behavior

As preliminary example, the well known equation provided by Eurocode 6 (1996) (see also

Brencich and Gambarotta 2005, Lourenço and Pina-Henriques 2006) for the evaluation of masonry compressive strength is considered

$$f_{ck} = K f_{cu}^{0.7} f_{cm}^{0.3} \quad (16)$$

where f_{ck} is the masonry compressive strength, f_{cu} is the unit compressive strength and f_{cm} is mortar compressive strength, while K is a constant which depends on the type of units and the type of masonry (in this example $K = 0.55$). We assume that f_{cu} and f_{cm} are independent Gaussian random variables, with mean and standard deviation (listed in Table 1) estimated from some experimental data reported by (Brencich and Gambarotta 2005) for eccentrically compressed masonry triplets. It is worth noting that Gaussian distributions obviously have infinite tails, which seems actually not physically reasonable (e.g., negative strength values are not permitted). However, they have been considered acceptable from an engineering point of view, since the occurrence probability of negative strength values is very close to zero, see Table 1.

It is worth noting that Eq. (16) relates masonry compressive strength f_{ck} with corresponding values of bricks and mortar, underlining that a complex interaction exists between constituent materials at failure. There are, indeed, physical limits inherent in the use of Eq. (16), consisting in the fact that compressive fracture energy is assumed as a non random parameter. It is well known, in fact, that masonry compressive failure is related to crushing, which is obviously a fragile phenomenon. However, the example at hand is here treated for its simplicity, since it provides an explicit formula for function $h(-)$, which allows a comparison between the true output probability distribution obtained by direct mathematical calculations (see Appendix A) and that estimated by MC simulations via fitted polynomial RS model.

For the present example, small MC and LH samples of size 20 are used to construct RS models; as an example, Fig. 5(a) shows the fitted RS model with the corresponding LH calibration points.

Fig. 6 and Fig. 7 show the mean and variance of the fitting errors calculated on 10 replicated MC-RS and LH-RS models, evaluated for each of the three MC samples of size 3000 used as validation points (mean and variance values for the other examples are also shown).

As can be seen, according to the error values, both MC-RS and LH-RS models seem to provide a comparable overall fitting performance. In fact, while for the RMSE the LH-RS models show a less mean error, but a greater variance with respect to MC-RS models, for MAE and MARE both MC-

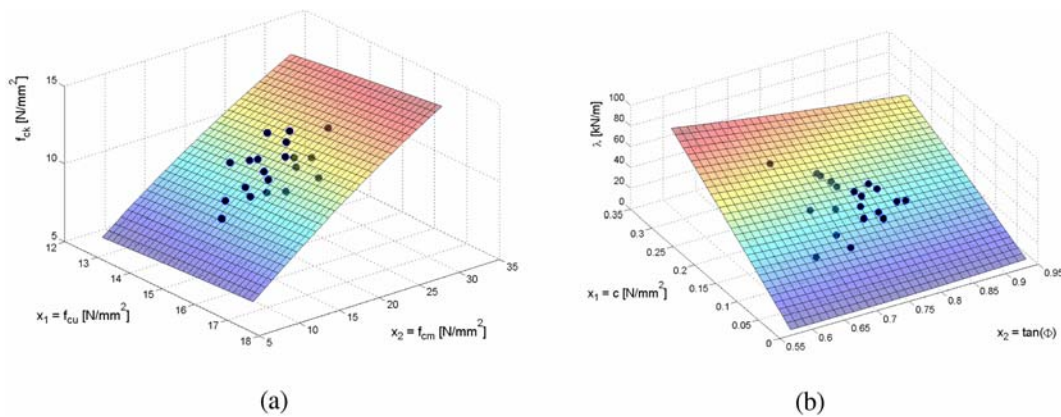


Fig. 5 Polynomial RS model with the 20 LH calibration points for (a) Example 1, (b) Example 2

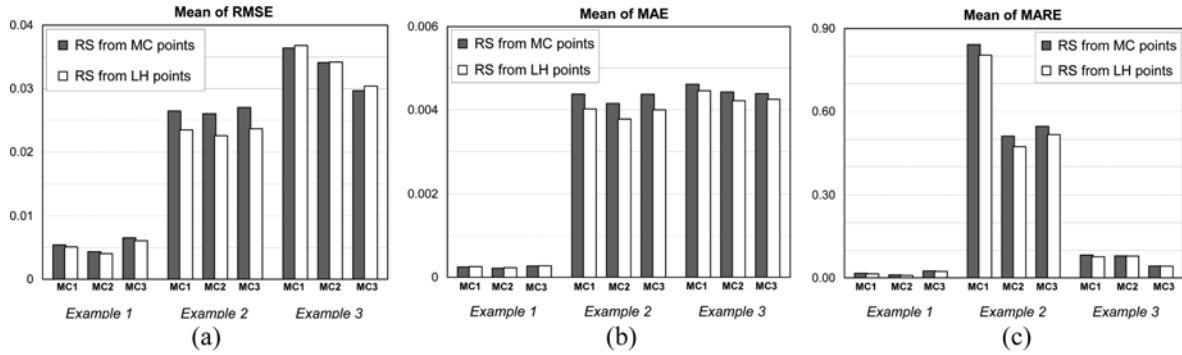


Fig. 6 Overall comparison of the mean of the fitting errors (RMSE, MAE, MARE) calculated on 10 replicated polynomial RS models constructed from MC and LH design points

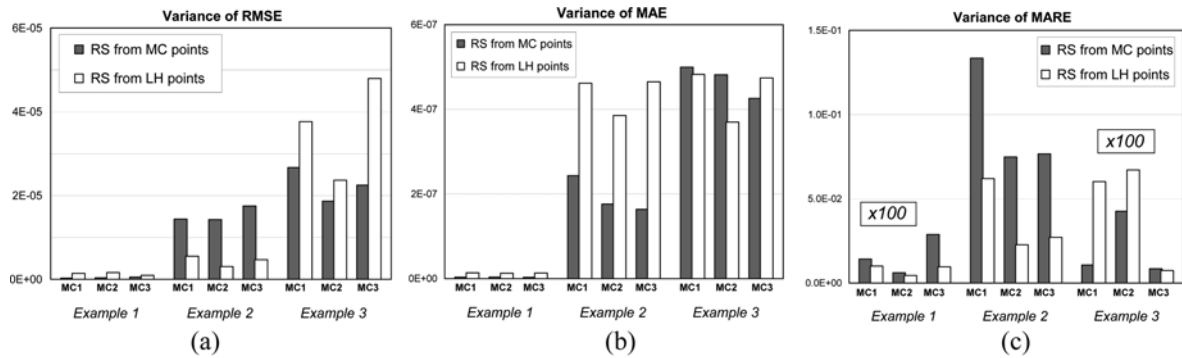


Fig. 7 Overall comparison of the variance of the fitting errors (RMSE, MAE, MARE) calculated on 10 replicated polynomial RS models constructed from MC and LH design points

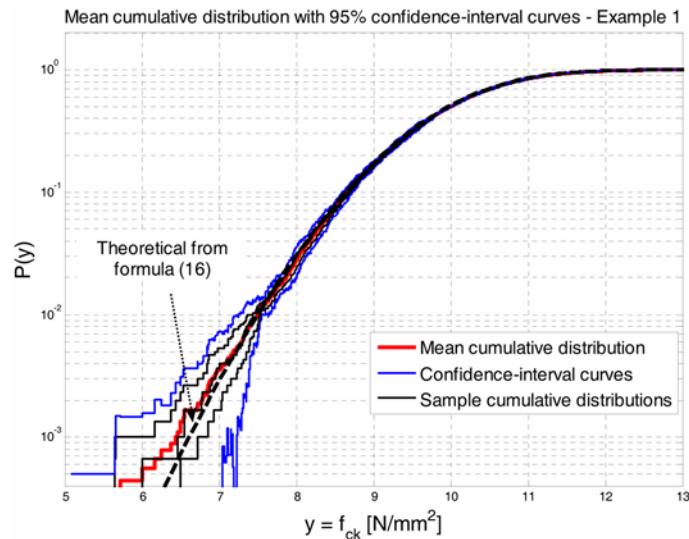


Fig. 8 Comparison of the empirical cumulative distribution from three replicated Monte Carlo samples of size 3000 with the mean empirical cumulative distribution and the 95% confidence-interval curves. The theoretical cumulative distribution is also shown (dashed line). Data refer to Example 1

RS and LH-RS models give comparable mean fitting errors, with LH-RS models showing instead a lower variance for MARE.

The three large MC samples of size 3000 previously taken as validation points to check RS fitting performance are also used to estimate the collapse load probability distribution, via direct computer simulations and via the estimated RS models. For what concerns the variability in the output probability distribution obtained from MC simulations, Fig. 8 compares (in logarithmic scale) the empirical cumulative distributions derived from the three MC simulations of size 3000 and the true distribution obtained as in Appendix A (the mean curve and the 0.95 confidence-interval curves are also shown). As the figure reveals, the empirical cumulative distribution $\hat{P}(y)$ is in quite good agreement with the true distribution $P(y)$, for sufficiently low probabilities (at least equal to or greater than 1%), while some scatter is observed for very low probabilities.

Finally, Fig. 9 (bottom) shows an overall comparison among output probability distributions: that

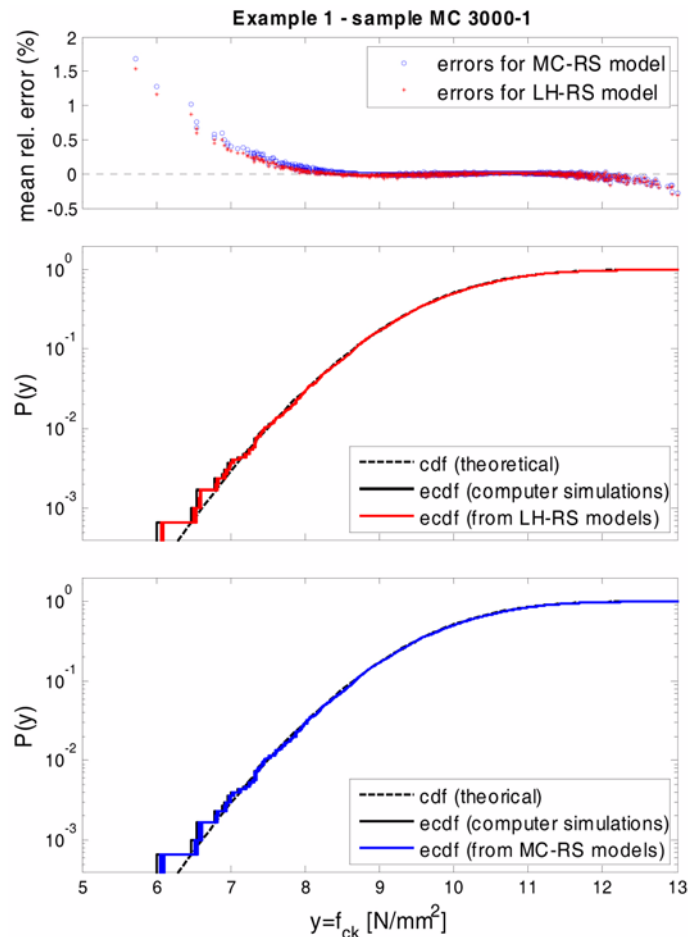


Fig. 9 Comparison of the empirical distribution functions obtained in large Monte Carlo simulations via direct computer simulations and via polynomial RS models. The theoretical cumulative distribution is also shown (dashed line). The average relative percentage error calculated on 10 replicated RS models is also shown. Data refer to Example 1

derived from computer simulations and that obtained from MC-RS and LH-RS polynomial RS models (the true cumulative probability density function derived in Appendix A is also added as a dashed line). Furthermore, in Fig. 9 the mean percentage relative error $err_i(\%)$ calculated on 10 replicated RS models is also reported. As can be seen, the cumulative distribution obtained via polynomial RS models is in general good agreement with the distribution obtained with direct computer simulations, except for the lower tails of the distribution, where we have larger errors. Furthermore, the mean $err_i(\%)$, which is used to detect the local fitting performance as a function of y_i values, shows that LH-RS models, compared to MC-RS ones, seem to provide lower prediction errors, especially for very low f_{ck} values. As it is possible to notice, for both RS models the maximum percentage error obtained is less than 2%, indicating the good performance of polynomial RS models, at least for this example.

As can be noted in Fig. 9, all the cumulative distributions obtained from RS models tend to be lower than the cumulative distributions provided by direct computer simulations. This effect can be correlated to the accuracy of RS models, which tends to be higher in the central region of the output probability distribution, while the prediction accuracy gets worse in the tails of the distribution (“tail reversal” effect, see Ramu *et al.* 2007); for instance, while for large f_{ck} values we have negative percentage errors (i.e., the RS model predicts lower value than the actual), in the left tail of the distribution we have positive errors (i.e., the RS model underestimates the actual analysis output). These negative errors can be attributed to the least-squares method used for fitting the polynomial RS model on calibration points, which minimizes the errors squared, rather than the absolute relative errors, assigning greater weights to the highest absolute output values. On the other hand, the largest errors occur only for very low f_{ck} values, for very small occurrence probabilities; in any case, the prediction errors become acceptable for probabilities at least greater than 5%.

3.2 Example 2: A real homogenized limit analysis problem

Let us consider two perpendicular masonry walls of dimensions $L_1 = 500$ cm, $L_2 = 300$ cm, $H = 300$ cm, $t = 30$ cm and with perfect interlocking, as shown in Fig. 10. Such walls are subjected to a constant vertical load due to typical dead and live loads assumed equal to $P_0 = 120$ N/mm and an increasing horizontal load depending on a load multiplier $y = \lambda$, simulating an equivalent static seismic action. Several homogenized limit analyses FE simulations are performed on the structure by means of the triangular discretization shown in Fig. 10(b). Masonry is supposed constituted by Italian common bricks of dimensions 250 mm \times 120 mm \times 55 mm disposed in running bond texture, with joints thickness equal to 10 mm.

We assume for joints a Mohr-Coulomb failure criterion with cohesion c and friction angle $\tan(\Phi)$ both modeled as independent normally distributed random variables, with mean and standard deviation (listed in Table 1) deduced from some experimental data reported in (van der Pluijm 1999).

At the opposite of Example 1, for this example no information is available on the input/output relationship $h(-)$, which makes impossible the explicit computation of the collapse load output probability distribution $P(y)$, estimated instead by extensive MC simulations.

As in the previous example, a polynomial RS model is constructed from either MC and LH sample sets of $n_c = 20$ points; more precisely, for each input pair $(c_i, \tan(\Phi))$, a 3D homogenized limit analysis is performed, so obtaining a set of n_c collapse loads y_i , used to construct a polynomial RS model. As an example, Fig. 5(b) shows the fitted RS model with the LH calibration points.

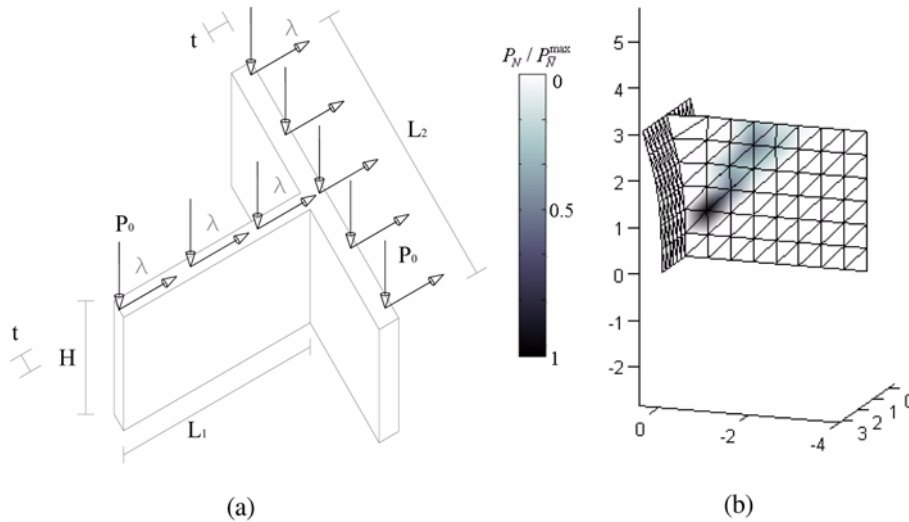


Fig. 10 Perpendicular masonry walls subjected to horizontal action used in Example 2 (a) geometry and (b) mesh used. A typical deformed shape at collapse obtained by means of the limit analysis FE procedure adopted is also reported (P_N is the in-plane plastic dissipation evaluated at node N and \bar{N} is the node of maximum dissipation)

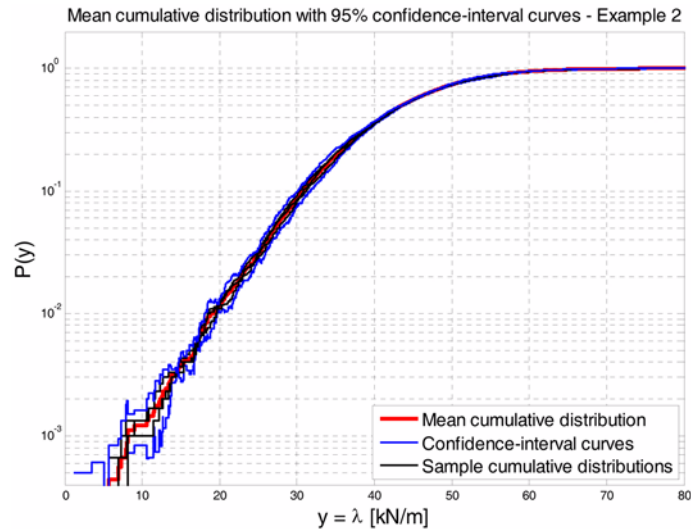


Fig. 11 Comparison of the empirical cumulative distribution from three replicated Monte Carlo samples of size 3000 with the mean empirical cumulative distribution and the 95% confidence-interval curves. Data refer to Example 2

The estimated RS model is then used as a proxy of direct computer finite element calculations in extensive MC simulations with 3000 sample points, used to assess the collapse load probability distribution. It is worth noting that each of the 3000 MC simulations required 37 h 27 min to be performed on an Intel Pentium 3 GHz PC equipped with 1GB RAM, whereas the construction of the polynomial RS model and the evaluation of the predicted output required only 12 min.

In Fig. 11 we show the variability in the collapse load empirical cumulative distribution obtained

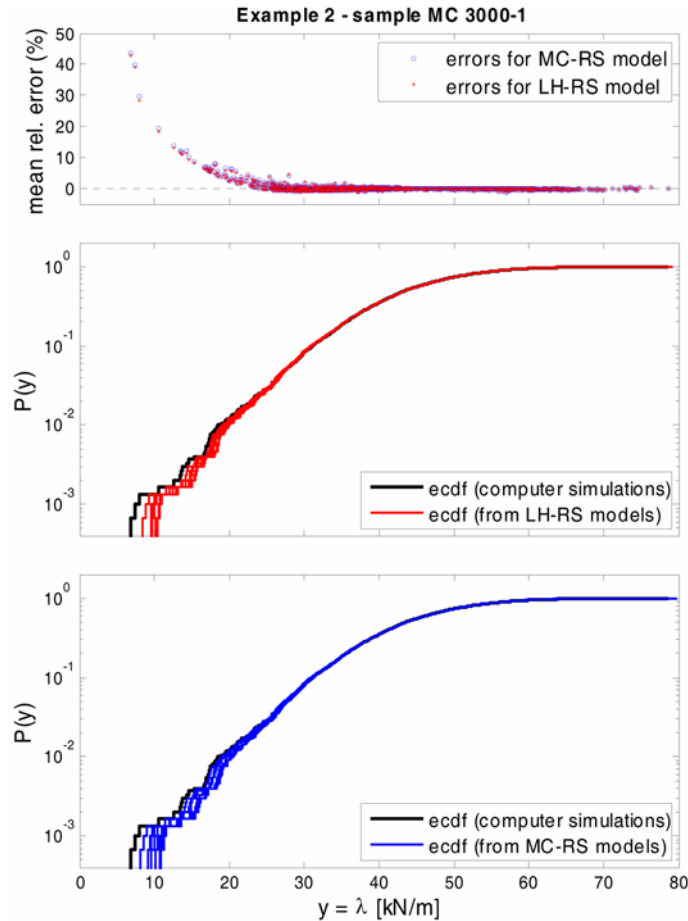


Fig. 12 Comparison of the empirical distribution functions obtained in large Monte Carlo simulations via direct computer simulations and via polynomial RS models. The theoretical cumulative distribution is also shown (dashed line). The average relative percentage error calculated on 10 replicated RS models is also shown. Data refer to Example 2

from the three 3000 MC computer simulations via direct computer calculations, compared with the mean probability distribution and the 95% confidence-interval curves. Compared to the previous example, a lower variability is observed. On the other hand, in Fig. 12, the probability distributions provided by direct computer simulations and via the estimated RS models are represented, as well the mean percentage prediction errors $err_i(\%)$ for the RS models are depicted. As it is possible to notice from Fig. 12, reported in logarithmic scale along the y -axis in order to amplify the phenomenon, the RS models are able to give reliable results approximately for probability greater than 1%, thus demonstrating that the proposed approach can be used for practical applications.

As already noted for Example 1, the probability distributions from RS models tend to be lower than those from direct MC simulations. This discrepancy for low collapse load values is easily justifiable by considering that, when collapse load tends to zero (i.e., when cohesion and friction angle of mortar joints are very low), a least-squares approximation used to calibrate the RS model tends to assign negligible optimization weights for low values of the collapse load (at least if such

weights are compared to those relative to high values of y). On the other hand, the prediction error becomes small (i.e., below 10%) for cumulated probabilities equal or greater of 1%, which seems acceptable in practical applications.

Finally, a comparison of the mean and variance of the error measures calculated on 10 replicated RS models are shown in Fig. 6 and Fig. 7. For this example, it seems quite clear how the overall prediction accuracy of LH-RS models is almost systematically better than that of MC-RS models. In particular, LH-RS models show both an overall better accuracy (in terms of RMSE and MAE) and a best local fitting performance, quantified by MARE. In addition, LH-RS models show a better accuracy for low y values, corresponding to the left-end tail of the collapse load distribution, as confirmed by the slightly lower mean percentage error observed for low y values (see top of Fig. 12).

3.3 Example 3: Shear masonry wall with mortar cohesion c , friction $\tan(\Phi)$ and tensile strength f_t assumed as random variables

Let the shear wall of Fig. 13 be considered, with dimensions $L = 600$ cm (length), $H = 300$ cm (height), $t = 45$ cm (thickness) and vertical load equal to 45 N/mm, corresponding to a low average compressive stress equal to 0.10 MPa. For the sake of simplicity, the wall is assumed build in stretcher bond with common Italian bricks of dimensions 250 mm \times 120 mm \times 55 mm infinitely resistant and joints reduced to interfaces with cohesive frictional behavior and limited tensile strength f_t , see Fig. 14.

In order to model both mortar tensile strength f_t , cohesion c and friction angle $\tan(\Phi)$ as independent random variables, the following model is assumed. While for the variability of cohesion c and $\tan(\Phi)$ we simply adopt two independent Gaussian distributions, with mean and standard deviation (see Table 1) estimated from some experimental data reported in (van der Pluijm 1999) (see Table 1), to represent the variability of f_t , the typical limitation $f_t \leq c/\tan(\Phi)$ must be included, see Fig. 14.

Since for each sampled pair $(c_i, \tan(\Phi))$ the maximum allowable f_t value must be always equal or

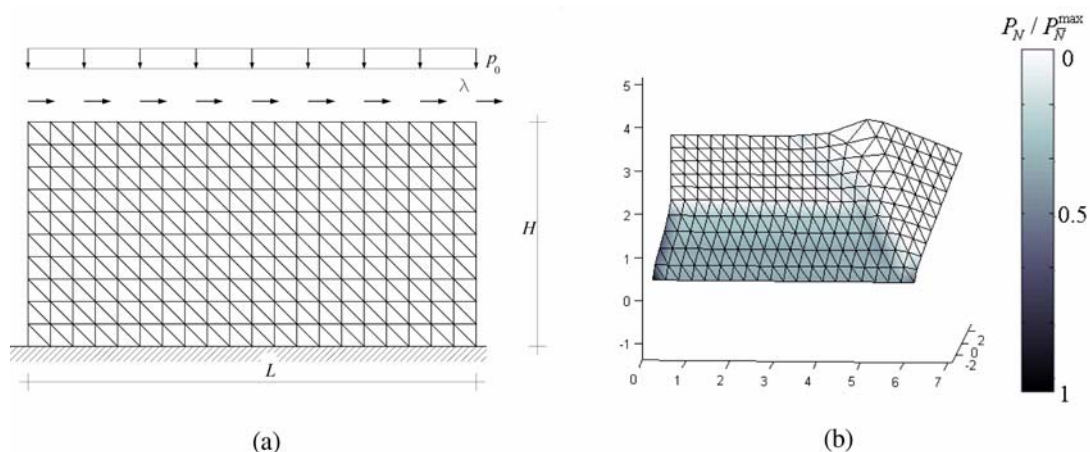


Fig. 13 (a) Shear wall tested and mesh used for the limit analysis FE simulations of Example 3, (b) Typical deformed shape at collapse obtained with the limit analysis FE model (P_N is the in-plane plastic dissipation evaluated at node N and \bar{N} is the node of maximum dissipation)

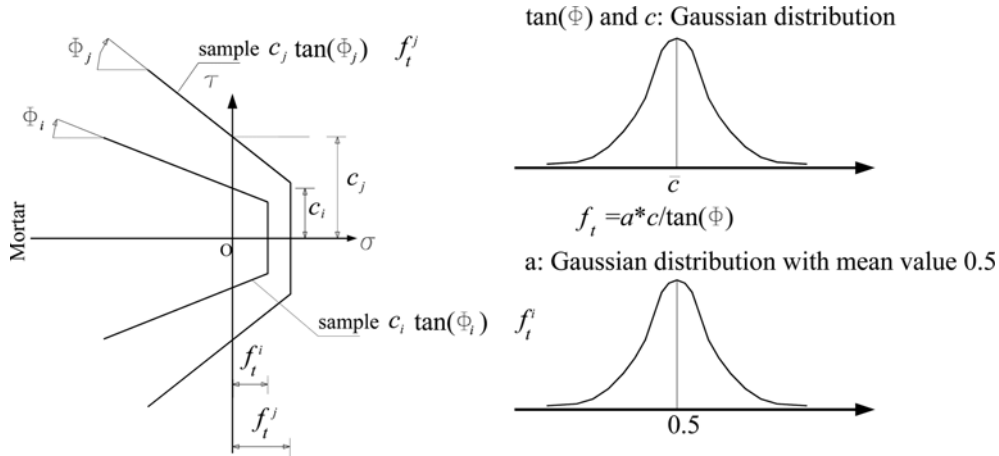


Fig. 14 Joints limit state domain obtained assuming two different sets i and j of random input parameters, Example 3

lower than the limit tensile strength $f_{t,lim}^i = c_i/\tan(\Phi_i)$, to define the variable f_t we introduce the following relationship

$$f_t = a \cdot \frac{c}{\tan(\Phi)} \tag{17}$$

where a is an auxiliary random variable following a normal distribution with mean and standard deviation reported in Table 1. When a sufficiently small standard deviation is used, as that of Table 1, possible inadmissibility of f_t is avoided from a technical point of view, i.e., a very limited number (<3-5) of points sampled do not respect the restriction $f_t \leq c/\tan(\Phi)$, a compromise which seems technically acceptable. Points which do not respect the constrain $f_t \leq c/\tan(\Phi)$ are discarded from the simulations. Furthermore, the mean and standard deviation of variable a are conveniently calibrated, so to obtain distribution parameters for f_t (see Appendix B) close to typical experimental data available in the literature, see Table 1.

As in the previous example, no information is available on the actual $\lambda(c, \tan(\Phi), f_t)$ input/output relationship, meaning that the true cumulative distribution $P(y)$ can be only approximated by extensive MC simulations. To this scope, the use of polynomial RS models as inexpensive replacement of direct computer calculations is investigated.

As described in Section 2, a quadratic polynomial RS model is constructed based on $n_c = 30$ calibration points generated by either the MC method or the LH technique. For each MC or LH input points $(c_i, \tan(\Phi_i), f_t^i)$, a 3D homogenized limit analysis is performed, so obtaining a set of n_c collapse loads y_i , used to fit the polynomial RS model. The fitted RS models are finally used in place of direct computer simulations in extensive MC simulations, to assess the output probability distribution.

Three large scale MC simulations with 1000 points are carried out both with direct computer simulations and via the estimated RS models, to compute a large set of outputs values y_i necessary for estimating the collapse load probability distribution. A mesh with 400 triangular three-noded elements is used for the simulations, as shown in Fig. 13. It is worth noting that each of the 1000 points MC simulations required approximately 12 hours to be performed on a Intel Pentium 3 GHz

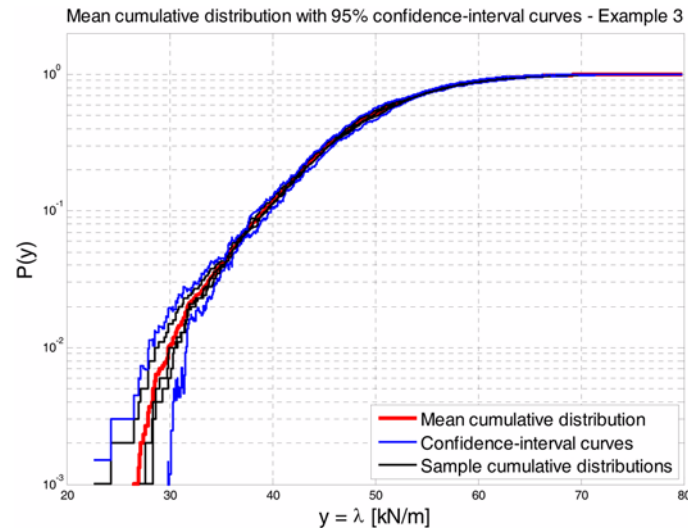


Fig. 15 Comparison of the empirical cumulative distribution from three replicated Monte Carlo samples of size 1000 with the mean empirical cumulative distribution and the 95% confidence-interval curves. Data refer to Example 3

PC equipped with 1GB RAM, immensely higher than the time required by the RS technique (20 minutes).

The variability in the cumulative distribution obtained from MC simulations with direct computer simulations is shown in Fig. 15. In this case, the scatter in the empirical distribution tends to greatly reduce for cumulated probabilities equal or greater than 2%.

The same three large MC samples are also used to assess the relative prediction accuracy of MC and LH polynomial RS models, by comparing the error metrics introduced in Section 2.5. We refer to Fig. 6 and Fig. 7 for the comparison of the mean and variance of the prediction errors, calculated on the 10 independent RS replicated models.

Contrarily to the previous examples, the present prediction errors seem to show opposite trends on the error estimators. While the mean of RMSE exhibits a slightly better accuracy for RS-MC models, the MAE says the opposite, while for MARE we have comparable errors. An exhaustive explanation of this apparent discrepancy is not an easy task. What is worth noting is that, while RMSE, MAE and MARE metrics provide a “global” performance of the LH-RS sampling, the relative percentage error gives a “local” estimation of the approximation performance. Indeed, the relative percentage errors reported in Fig. 16 shows a fairly better accuracy of LH polynomial RS models in the region of low collapse load values (compare, for instance errors provided by MC and LH for collapse loads lower than 30 kN/m), which is the range of engineering interest.

4. Critical remarks

As emphasized by the results presented in the preceding Section, the use of RS technique as a proxy of direct computer simulations in extensive MC simulations provides a significant reduction in the overall computation time, while assuring at the same time a sufficient level of accuracy.

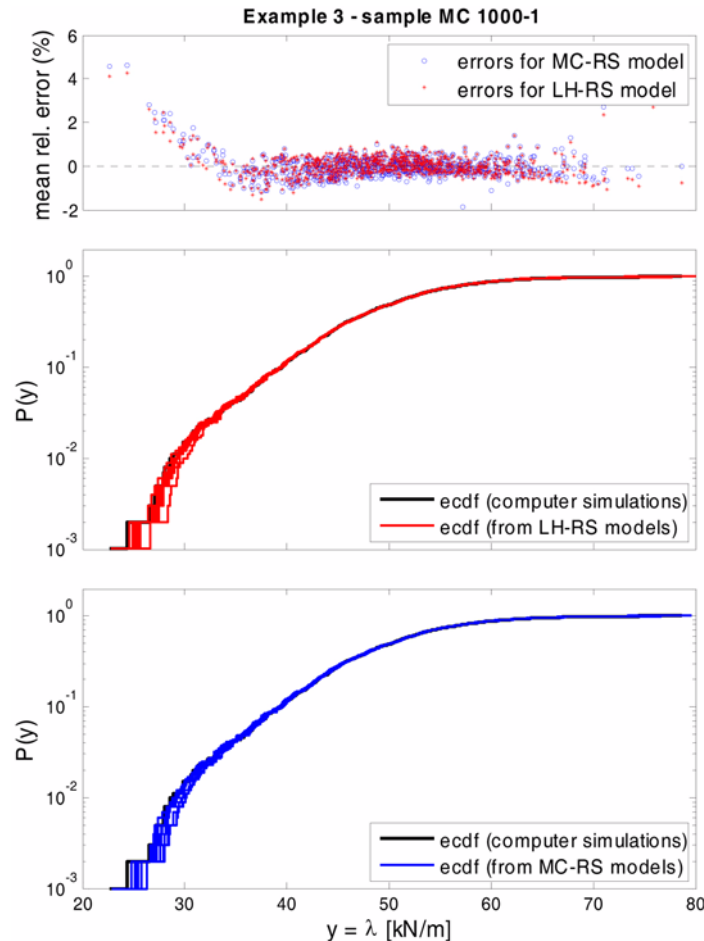


Fig. 16 Comparison of the empirical distribution functions obtained in large Monte Carlo simulations via direct computer simulations and via polynomial RS models. The theoretical cumulative distribution is also shown (dashed line). The average relative percentage error calculated on 10 replicated RS models is also shown. Data refer to Example 3

For what concerns RS prediction accuracy, in general LH-RS models seem to provide a better accuracy than MC-RS models. More precisely, while the overall prediction accuracy quantified by RMSE seems comparable, the local fitting performance quantified by MARE and, in particular, by $err_i(\%)$ seems better for LH-RS models, especially for low y values, which is particularly important when accurate estimates of the left-end tail of the collapse load probability distribution (associated to low probability levels) are requested.

A second aspect which has been emphasized by our analysis is the uncertainty which affects the output probability distribution $P(y)$ estimated in extensive MC simulations with direct computer simulations. In particular, the uncertainty in output probability distribution is evident in the distribution tails, where MC samples of the output variable y are scarcely populated, although for probabilities larger than 1% the estimation error becomes very small.

Of greater interest, instead, is the evaluation of the prediction performance of fitted RS models with respect to results provided by direct computer calculations in extensive MC simulations. Due

to the least-square method used to fit polynomial RS models, positive percentage relative errors have been observed for low output values, which determines a decrease in the performance of RS models in cumulative distribution assessment. More specifically, when considering the extensive MC simulations the probability distributions obtained through RS models tend to be lower than those calculated from direct computer simulations. On the other hand, for cumulated probabilities at least equal or greater than 5%, the prediction error becomes acceptable for practical applications, indicating that the RS models give sufficiently accurate estimations of the collapse load probability distribution for the range of practical interest, providing at the same time a drastic reduction in the overall computational time.

To conclude, it is worth noting how further improvements on the prediction capability of fitted RS models might be achieved by using other approximating models (Simpson *et al.* 2001 and, e.g., non-parametric regression Storlie and Helton 2008a, b, Storlie *et al.* 2009) different from simple polynomial regression, even though at the expense of an increase in metamodel complexity.

5. Conclusions

A methodology based polynomial RS models has been used as an alternative to direct computer calculations in extensive MC simulations, used to assess the collapse load probability distribution of masonry structures having random input parameters.

The correlation between RS accuracy and sampling technique used to generate small sets of input calibration points is tested by comparing the MC with the LH method, which is sought to provide more effective input variable coverage. The relative prediction accuracy of MC and LH polynomial RS models is quantified by calculating appropriate fitting errors at additional validation points.

The fitted RS models have been used in extensive MC simulations in place of actual computer calculations, to estimate the collapse load probability distribution.

The procedure has been tested on three different examples of technical interest and several comparisons of the estimated collapse load distributions obtained with direct expensive MC simulations have been reported.

It can be concluded that:

- in the framework of stochastic homogenized limit analysis, the polynomial RS models have shown to give accurate estimations in a technically meaningful region of the output domains inspected, while providing a drastic reduction in the overall computation time, compared to that required by direct computer calculations;
- the approach with polynomial RS models only needs MC and LH simulations with few points (<30), instead of expensive (>1000 points) MC simulations performed via direct calculations;
- The presented analyses have shown that RS model may represent a valuable tool for a fast estimation of collapse load distribution of real scale masonry buildings, where large MC computer simulations need a prohibitive computational time (>40 hours), thus being not feasible in engineering practice. A validation of this statement is obviously needed case by case. On the other hand, a work in progress activity by the authors is to analyze the performance of the approach proposed generalizing the problem to multiple uncertain inputs (more than 3).

References

- Apostolakis, G. (1990), "The concept of probability in safety assessments of technological systems", *Science*, **250**(4986), 1359-1364.
- Bicanic, N., Stirling, C. and Pearce, C.J. (2003), "Discontinuous modelling of masonry bridges", *Comput. Mech.*, **31**, 60-68.
- Brenchi, A. and Gambarotta, L. (2005), "Mechanical response of solid clay brickwork under eccentric loading. Part I: Unreinforced masonry", *Mater. Struct.*, **38**(276), 257-266.
- Eurocode 6 (1996), *Design of Masonry Structures*, EN 1996.
- Florian, A. (1992), "An efficient sampling scheme: Updated Latin Hypercube sampling", *Probabilist, Eng. Mech.*, **7**, 123-130.
- Giunta, A.A. and Watson, L.T. (1998), "A comparison of approximation modeling techniques: polynomial versus interpolating models", *Proceedings of the 7th AIAA/USAF/NASA/ISSMO Symposium on Multidisciplinary Analysis and Optimization*, St. Louis, September.
- Giunta, A.A., Wojtkiewicz, S.F. and Eldred, M.S. (2003), "Overview of modern design of experiments methods for computational simulations", *Proceedings of the 41st AIAA, Aerospace Sciences Meeting and Exhibit*, Reno, January.
- Glynn, P.W. and Iglehart, D.L. (1989), "Importance sampling for stochastic simulations", *Manage. Sci.*, **35**(11), 1367-1392.
- Goodman, L.A. (1960), "On the exact variance of products", *J. Am. Stat. Assoc.*, **55**(292), 708-713.
- Goyal, A., Shahabuddin, P., Heidelberger, P., Nicola, V.F. and Glynn, P.W. (1992), "A unified framework for simulating Markovian models of highly dependable systems", *IEEE T. Comput.*, **41**(1), 36-51.
- Haan, C.T. (1989), "Parametric uncertainty in hydrologic modeling", *Trans. ASAE*, **32**(1), 137-146.
- Heidelberger, P. (1995), "Fast simulation of rare events in queueing and reliability models", *ACM T. Model. Comput. Simul.*, **5**(1), 43-85.
- Helton, J.C. (1994), "Treatment of uncertainty in performance assessments for complex systems", *Risk Anal.*, **14**(4), 483-511.
- Helton, J.C. (1997), "Uncertainty and sensitivity analysis in the presence of stochastic and subjective uncertainty", *J. Stat. Comput. Simul.*, **57**(1-4), 3-76.
- Helton, J.C. and Burmaster, D.E. (1996), "Guest editorial: treatment of aleatory and epistemic uncertainty in performance assessments for complex systems", *Reliab. Eng. Syst. Safe.*, **54**(2-3), 91-94.
- Helton, J.C. and Davis, F.J. (2003), "Latin Hypercube and the propagation of the uncertainty in analyses of complex systems", *Reliab. Eng. Syst. Safe.*, **81**, 23-69.
- Helton, J.C., Davis, F.J. and Johnson, J.D. (2005), "A comparison of uncertainty and sensitivity analysis results obtained with random and Latin Hypercube sampling", *Reliab. Eng. Syst. Safe.*, **89**(3), 305-330.
- Hoffman, F.O. and Hammonds, J.S. (1994), "Propagation of uncertainty in risk assessments: the need to distinguish between uncertainty due to lack of knowledge and uncertainty due to variability", *Risk Anal.*, **14**(5), 707-712.
- Hradil, P., Žak, J., Novák, D. and Lavicky, D. (2001), "Stochastic analysis of historical masonry structures", *Hist. Construct.*, Lourenço P.B., Roca, P. (eds), Guimarães.
- Huntington, D.E. and Lyrantzis, C.S. (1998), "Improvements to and limitations of Latin Hypercube sampling", *Probabilist, Eng. Mech.*, **13**(4), 245-253.
- Iman, R.L. (1981), "Statistical methods for including uncertainties associated with the geologic isolation of radioactive waste which allow for a comparison with licensing criteria", *Proceedings of the Symposium on Uncertainties Associated with the Regulation of the Geologic Disposal of High-Level Radioactive Waste* (Ed. Kocher, D.C.), Gatlinburg, March.
- Jin, R., Chen, W. and Simpson, T.W. (2001), "Comparative studies of metamodelling techniques under multiple modeling criteria", *Struct. Multidiscip. O.*, **23**, 1-13.
- Krabbenhoft, K., Lyamin, A.V., Hija, M. and Sloan, S.W. (2005), "A new discontinuous upper bound limit analysis formulation", *Int. J. Numer. Meth. Eng.*, **63**, 1069-1088.
- Lofli, H.R. and Shing, B.P. (1994), "Interface model applied to fracture of masonry structures", *J. Struct. Eng.*, **120**, 63-80.

- Lourenço, P.B., de Borst, R. and Rots, J.G. (1997), "A plane stress softening plasticity model for orthotropic materials", *Int. J. Numer. Meth. Eng.*, **40**, 4033-4057.
- Lourenço, P.B. (1999), "Anisotropic softening model for masonry plates and shells", *J. Struct. Eng.*, **126**(9), 1008-1016.
- Lourenço, P.B. and Pina-Henriques, J. (2006), "Validation of analytical and continuum numerical methods for estimating the compressive strength of masonry", *Comput. Struct.*, **84**(29-30), 1977-1989.
- Magenes, G. and Calvi, G.M. (1997), "In-plane seismic response of brick masonry walls", *Earth. Eng. Struct. D.*, **26**, 1091-1112.
- McKay, M.D., Conover, W.J. and Beckman, R.J. (1979), "A comparison of three methods for selecting values of input variables in the analysis of output from a computer code", *Technometrics*, **21**, 239-245.
- Melchers, R.E. (1990), "Search-based importance sampling", *Struct. Safe.*, **9**(2), 117-128.
- Milani, G., Lourenço, P.B. and Tralli, A. (2006a), "Homogenization approach for the limit analysis of out-of-plane loaded masonry walls", *J. Struct. Eng.*, **132**(10), 1650-1663.
- Milani, G., Lourenço, P.B. and Tralli, A. (2006b), "Homogenised limit analysis of masonry walls. Part I: failure surfaces", *Comput. Struct.*, **84**, 166-180.
- Milani, G., Lourenço, P.B. and Tralli, A. (2006c), "Homogenised limit analysis of masonry walls. Part II: structural examples", *Comput. Struct.*, **84**, 181-195.
- Milani, G., Lourenço, P.B. and Tralli, A. (2007a), "3D homogenized limit analysis of masonry buildings under horizontal loads", *Eng. Struct.*, **29**(11), 3134-3148.
- Milani, G., Zuccarello, F.A., Olivito, R.S. and Tralli, A. (2007b), "Heterogeneous upper-bound finite element limit analysis of masonry walls out-of-plane loaded", *Comput. Mech.*, **40**(6), 911-931.
- Mood, A., Graybill, F. and Boes, D. (1974), *Introduction to the Theory of Statistics*, McGraw-Hill.
- Neves, R.A., Chateaufneuf, A., Venturini, W.S. and Lemaire, M. (2006), "Reliability analysis of reinforced concrete grids with nonlinear material behavior", *Reliab. Eng. Syst. Safe.*, **91**, 735-744.
- Nicola, V.F., Shahabuddin, P. and Nakayama, M.K. (2001), "Techniques for fast simulation of models of highly dependable systems", *IEEE T. Reliab.*, **50**(3), 246-264.
- Olsen, P.C. (1999), "Evaluation of triangular elements in rigid-plastic finite element analysis of reinforced concrete", *Comput. Meth. Appl. Mech. Eng.*, **179**, 1-17.
- Olsen, P.C. (2001), "Rigid-plastic finite element analysis of steel plates, structural girders and connections", *Comput. Meth. Appl. Mech. Eng.*, **191**, 761-781.
- Owen, A. and Zhou, Y. (2000), "Safe and effective importance sampling", *J. Am. Stat. Assoc.*, **95**(449), 135-143.
- Parry, G.W. and Winter, P.W. (1981), "Characterization and evaluation of uncertainty in probabilistic risk analysis", *Nucl. Safe.*, **22**(1), 28-42.
- Paté-Cornell, M.E. (1996), "Uncertainties in risk analysis: six levels of treatment", *Reliab. Eng. Syst. Safe.*, **54**(2-3), 95-111.
- Pendola, M., Mohamed, A., Lemaire, M. and Hornet, P. (2000), "Combination of finite element and reliability methods in nonlinear fracture mechanics", *Reliab. Eng. Syst. Safe.*, **70**, 15-27.
- Ramu, P., Kim, N.H. and Haftka, R.T. (2007), "Error amplification in failure probability estimates due to small errors in response surface", SAE paper 2007-01-0549.
- Sejnoha, J., Sejnoha, M., Zeman, J., Sykora, J. and Vorel, J. (2008), "Mesoscopic study on historic masonry", *Struct. Eng. Mech.*, **30**(1), 99-117.
- Shahabuddin, P. (1994), "Importance sampling for the simulation of highly reliable Markovian systems", *Manage. Sci.*, **40**(3), 333-352.
- Simpson, T.W., Peplinski, J.D., Koch, P.N. and Allen, J.K. (2001), "Metamodels for Computer-based Engineering Design: Survey and recommendations", *Eng. Comput.*, **17**, 129-150.
- Simpson, T.W., Lin, D.K.J. and Chen, W. (2002), "Sampling strategies for computer experiments: design and analysis", *Int. J. Rel. Appl.*, **2**(3), 209-240.
- Sloan, S.W. and Kleeman, P.W. (1995), "Upper bound limit analysis using discontinuous velocity fields", *Comput. Meth. Appl. Mech. Eng.*, **127**(1-4), 293-314.
- Storlie, C.B. and Helton, J.C. (2008a), "Multiple predictor smoothing methods for sensitivity analysis: description of techniques", *Reliab. Eng. Syst. Safe.*, **93**(1), 28-54.
- Storlie, C.B. and Helton, J.C. (2008b), "Multiple predictor smoothing methods for sensitivity analysis: example

- results”, *Reliab. Eng. Syst. Safe.*, **93**(1), 55-77.
- Storlie, C.B., Swiler, L.P., Helton, J.C. and Sallaberry, C.J. (2009), “Implementation and evaluation of nonparametric regression procedures for sensitivity analysis of computationally demanding models”, *Reliab. Eng. Syst. Safe.*, **94**(11), 1735-1763.
- Suquet, P. (1983), “Analyse limite et homogenisation”, *CR Acad. Sci.*, **296**, 1355-1358 (in French).
- Sutcliffe, D.J., Yu, H.S. and Page, A.W. (2001), “Lower bound limit analysis of unreinforced masonry shear walls”, *Comput. Struct.*, **79**, 1295-1312.
- Swiler, L.P., Slepoy, R. and Giunta, A.A. (2006), “Evaluation of sampling methods in constructing response surface approximations”, *Proceedings of 47th AIAA/ASME/ASCE/AHS/ASC Structures, Structural Dynamics and Materials Conference*, Newport, Rhode Island.
- van der Pluijm, R. (1999), *Out-of-plane Bending of Masonry. Behaviour and Strength*, PhD Thesis, Eindhoven University of Technology.
- Vermeltoort, A. (2006), *Brick-mortar Interaction in Masonry Under Compression*, PhD Thesis, Eindhoven University of Technology.
- Winkler, R.L. (1996), “Uncertainty in probabilistic risk assessment”, *Reliab. Eng. Syst. Safe.*, **54**(2-3), 127-132.
- Yu, X. and Tin-Loi, F. (2006), “A simple mixed finite element for static limit analysis”, *Comput. Struct.*, **84**, 1906-1917.

Notations

a	: auxiliary Gaussian random variable
c	: cohesion
f_{ck}	: masonry compressive strength
f_{cu}	: units compressive strength
f_{cm}	: mortar compressive strength
f_t	: mortar tensile strength
$f_{t,lim} = c/\tan(\Phi)$: limit mortar tensile strength
$h(-)$: true input/output relationship
$\hat{h}(-)$: approximation of $h(-)$
LH-RS	: polynomial RS model constructed from Latin Hypercube points
MC-RS	: polynomial RS model constructed from Monte Carlo points
MAE	: Mean Absolute Error
MARE	: Maximum Absolute Relative Error
n	: number of large Monte Carlo simulations (1000 or 3000)
n_c	: number of calibration points (20 or 30)
$p(y)$: probability density function
$P(y)$: cumulative probability distribution
$\hat{P}(y)$: empirical cumulative distribution
$\bar{P}(y)$: mean empirical cumulative distribution
RMSE	: Root Mean Square Error
\bar{x}_i, σ_i	: mean and standard deviation of random input variable x_i
$\mathbf{x} = (x_1, x_2, \dots, x_m)$: random analysis inputs (material parameters)
$\mathbf{x}_{c,k}$: k th set of input calibration points for RS construction
y	: analysis output (collapse load)
y_i	: i th analysis output from direct computer simulation
$y_{p,i}$: i th analysis output estimated from polynomial RS model
$y_{c,k} = h(\mathbf{x}_{c,k})$: k th output value used in RS calibration
λ	: load multiplier
σ_p	: standard deviation of empirical distributions sample
$\tan(\Phi)$: tangent of friction angle

Appendix A – Theoretical output probability distribution for Example 1

The true probability distribution of the collapse load $y = h(x_1, x_2)$ which is a function of two random variables x_1 and x_2 can be calculated as (Mood *et al.* 1974)

$$p(y) = \int_0^{+\infty} p(x_1, x_2) \left| \frac{\partial x_1}{\partial y} \right| dx_2 \quad (18)$$

where $p(x_1, x_2)$ is the joint probability distribution function of $x_1 = h^{-1}(y, x_2)$ and x_2 . By referring to Example 1, where function $h(-)$ is given by Eq. (16), we have

$$x_1 = \left(\frac{y}{Kx_2^{0.3}} \right)^{\frac{1}{0.7}} \quad (19)$$

and therefore the derivative appearing in Eq. (18) becomes

$$\left| \frac{\partial x_1}{\partial y} \right| = \left| \frac{1}{0.7y} \left(\frac{y}{Kx_2^{0.3}} \right)^{\frac{1}{0.7}} \right| \quad (20)$$

Assuming now x_1 and x_2 as independent Gaussian variables (with mean \bar{x}_1, \bar{x}_2 and standard deviation σ_1, σ_2 , respectively), after some simplifications we obtain

$$p(y) = \frac{C}{ay} \cdot \int_0^{\infty} x_1 \exp \left[-\frac{\sigma_2^2 x_1 (x_1 - 2\bar{x}_1) + \sigma_1^2 x_2 (x_2 - 2\bar{x}_2)}{2\sigma_1^2 \sigma_2^2} \right] dx_2 \quad (21)$$

where x_1 is given by Eq. (19), while

$$C = \frac{1}{2\pi\sigma_1\sigma_2} \exp \left(-\frac{\bar{x}_1^2 \sigma_2^2 + \bar{x}_2^2 \sigma_1^2}{2\sigma_1^2 \sigma_2^2} \right) \quad (22)$$

Appendix B – Mean and standard deviation for cut-off stress in Example 3

This Appendix shows how to compute the mean and standard deviation of variable f_i , introduced in Example 3 and defined by Eq. (17). First, the probability density function for the limit tensile strength $f_{i,\text{lim}} = c/\tan(\Phi)$ is computed similarly to Appendix A

$$p_{f_{i,\text{lim}}}(y) = C \cdot \int_0^{\infty} |x_2| \exp \left[-\frac{(\sigma_1^2 + \sigma_2^2 y^2)x_2^2 - 2(\bar{x}_1 \sigma_2^2 y + \bar{x}_2 \sigma_1^2)x_2}{2\sigma_1^2 \sigma_2^2} \right] dx_2 \quad (23)$$

where C is defined in Eq. (22), while \bar{x}_1, \bar{x}_2 and σ_1, σ_2 are the mean and standard deviations of variables $x_1 = c$ and $x_2 = \tan(\Phi)$, respectively. Once the probability density function $p_{f_{i,\text{lim}}}(y)$ has been calculated according to Eq. (23), we can compute the mean value and standard deviation of $f_{i,\text{lim}}$, which are equal to $\bar{x}_{f_{i,\text{lim}}} = 0.1896$ [N/mm²] and $\sigma_{f_{i,\text{lim}}} = 0.0497$ [N/mm²], respectively.

Now, since $f_{i,\text{lim}}$ and $x_3 = a$ are assumed as independent random variables, the mean value and standard deviation for f_i are simply (Goodman 1960)

$$\begin{cases} \bar{x}_{f_i} = \bar{x}_{f_{i,\text{lim}}}\bar{x}_3 = 0.0948 \text{ [N/mm}^2\text{]} \\ \sigma_{f_i} = \sqrt{\bar{x}_3^2 \sigma_{f_{i,\text{lim}}}^2 + \bar{x}_{f_{i,\text{lim}}}^2 \sigma_3^2 + \sigma_{f_{i,\text{lim}}}^2 \sigma_3^2} = 0.0258 \text{ [N/mm}^2\text{]} \end{cases} \quad (24)$$

where symbols \bar{x}_3, σ_3 indicate the mean and the standard deviation of variable $x_3 = a$ (see Table 1).